EFFECTIVENESS OF LOW-SALINITY AND CO_2 FLOODING HYBRID APPROACHES IN LOW-PERMEABILITY SANDSTONE RESERVOIRS

A Thesis

by

HARISH T. KUMAR

Submitted to the Office of Graduate and Professional Studies of
Texas A&M University
in partial fulfillment of the requirements for the degree of

MASTER OF SCIENCE

Chair of Committee,	Hisham A. Nasr-El-Din
Committee Members,	Maria A. Barrufet
	Mahmoud El-Halwagi
Head of Department,	A. Daniel Hill

August 2016

Major Subject: Petroleum Engineering

ABSTRACT

Low-salinity waterflooding (LSW) has been an emerging Enhanced Oil Recovery (EOR) technique. LSW-alternating-CO_2 injection has recently proven to be a particularly strong EOR stimulation technique. Limited simulation studies have been performed to properly exhibit the interpretation of experimental studies in this area. This study aims to expand the interpretation and application of LSW in sandstone formations.

Low-permeability sandstones of 18% clay content, and medium west Texas crude oil with 29 °API, were selected for evaluating the potentials of LSW and CO_2 flooding. Coreflood experiments were conducted and interpreted by reservoir simulation, which enabled a better understanding of the underlying science of the studied EOR techniques. Five secondary waterflooding experiments and two LSW-CO_2 hybrid processes were performed using aged 3 in. outcrop Grey Bandera sandstone cores. The wettability of the rock was tested using axisymmetric contact angle measurements to study the effect of injected brine salinity. The interfacial tension values were measured for the different brines and medium crude oil systems. The corefloods were interpreted using reservoir simulation by history-matching the experimental oil RF (Recovery Factor) and the pressure drop across the core. A detailed focus was laid on interpretation of SCAL (Special Core Analyses) relative permeability curves for the various waterflooding operations, by comparing curves generated from published correlations, history-matched curves by simulation, and that by Corey's correlations.

Fines migration and viscosity override of low-salinity waters over medium oil influenced the oil recovery profile during LSW. Wettability alteration proved to be

effective during LSW for longer injection and production periods. Corey's exponents were found to be premature indications of rock wettability during LSW, proving the importance and reliability of experimental wettability characterization. Low-salinity waterflooding proved to be marginally effective over conventional waterflooding for sandstones with high clay contents and low permeabilities. Low-permeability sandstone reservoirs proved to be suitable targets for hybrid EOR techniques using CO_2 and LSW.

DEDICATION

This thesis is dedicated to my parents, sister, and grandmother.

ACKNOWLEDGEMENTS

I thank my committee chair, Dr. Hisham A. Nasr-El-Din, for his esteemed guidance and support to me during my period of study at Texas A&M University, and also particularly for his interest and care in my welfare. His constant motivation is highly responsible for my success.

I thank my committee member, Dr. Maria A. Barrufet, who imparted her experience and knowledge, and cleared all the doubts I had during my research. Her continuous guidance gave me great confidence in my work.

I thank my committee member, Dr. Mahmoud El-Halwagi, for agreeing to be a part of my committee, and for his constant encouragement.

I am grateful to all my professors in the Harold Vance Department of Petroleum Engineering at Texas A&M University for the guidance I have received in my courses. I have truly achieved my goal to become a good petroleum engineer based on their teachings.

Finally, I would like to thank all my friends for their constant support and backing during difficult times. My special thanks to Dr. Ahmed Shehata (former graduate student, Dr.Nasr-El-Din's group), for his invaluable friendship and motivation, Kristina Hansen (former member of Dr.Nasr-El-Din's group) and Gia Alexander (member of Dr.Nasr-El-Din's group), for their tremendous help in reviewing my work.

I also express my gratitude to the technical support teams of Schlumberger's Eclipse Reservoir Simulation Suite (2014.1) and Calsep's PVTSim (1.1.23 2016) Fluid Package.

NOMENCLATURE

CO_2	Carbon Dioxide
N_2	Nitrogen
EOR	Enhanced Oil Recovery
IOR	Improved Oil Recovery
WAG	Water-Alternating Gas
LSW	Low-Salinity Waterflooding
RF	Recovery Factor (%)
SCAL	Special Core Analyses
EDL	Electric Double Layer
MIE	Multi-Component Ion Exchange
ppm	Parts Per Million
TDS	Total Dissolved Solids
Kr	Relative Permeability
Kabs	Absolute Permeability (md)
Pc	Capillary Pressure (psi)
1-D	One-Dimensional
2-D	Two-Dimensional
Keo	Effective Permeability To Oil Phase (md)
Kew	Effective Permeability To Water Phase (md)
Kro	Relative Permeability To Oil Phase
Krw	Relative Permeability To Water Phase

Kro*	Normalized Relative Permeability To Oil Phase
Krw*	Normalized Relative Permeability To Water Phase
Sw	Water Saturation (fraction)
Sw*	Normalized Water Saturation (fraction)
No	Corey's Oil Curve Exponent
Nw	Corey's Water Curve Exponent
rpm	Revolutions Per Minute
IFT	Inter-Facial Tension (mN/m)
HP/HT	High Pressure / High Temperature
P_{max}	Maximum Pressure (psi)
DI	De-Ionized
XRD	X-Ray Diffraction
DSA	Drop Shape Analyzer
Swc	Connate Water Saturation (fraction)
Swirr	Irreducible Water Saturation (fraction)
Slr	Residual Liquid Saturation To Gas Flooding (fraction)
OOIP	Original Oil In Place (cm^3)
EOS	Equation Of State
E100	Eclipse Black Oil Reservoir Simulator (2014.1)
PV	Pore Volume (cm^3)
Sorw	End Point Residual Oil Saturation (fraction)
kbase	Base Permeability Value For Relative Permeability Curves (md)

μ_o	Oil Viscosity (cp)
Φ	Porosity (%)
μ_w	Water Viscosity (cp)

TABLE OF CONTENTS

Page

Page

LIST OF FIGURES

Page

Page

Page

LIST OF TABLES

Page

1. INTRODUCTION AND LITERATURE REVIEW

After pressure depletion, waterfloods have been a common way of secondary oil recovery. Formation water and seawater are the most commonly used injection fluids for this purpose. However in each of these cases, the full potential of the reservoir is not tapped. In this regard, methods for tertiary recovery, such as low-salinity water and CO_2 flooding are carried out. The following subsections outline the parameters of several factors that affect the success of such a recovery process.

Formation water has an average salt concentration, total dissolved solids (TDS), of about 100,000 ppm or greater. This is a very high saline water type, which originally exists in the reservoir in small or large saturations, from the time the reservoir came to exist. Seawater has a lower TDS of about 50,000 ppm on an average. Low-salinity water is generally considered to have salt concentrations under 30,000 ppm. These different salinities of injected water have marginal or major effects on improving the oil recovery, depending on the formation type and properties.

CO_2 is a fluid that has properties which facilitate the recovery of oil, under certain ambient conditions. It is a gas under normal temperature and pressure conditions. However, when injected into the formation, at high pressure and temperature conditions, it takes the form of a supercritical fluid. This CO_2's supercritical state is of benefit to the oil industry because it has properties such as density, which is almost identical to that of crude oil. This enables the CO_2 to mix well with the crude, due to similar consistency. Eventually, the resulting fluid from this mixture has physical properties contributing to ease in oil flow, thus enhancing the oil recovery. During CO_2

flooding operations, when the pressure conditions in the reservoir are considerably low, the CO_2 will not attain the supercritical state below a particular threshold value known as the Minimum Miscibility Pressure (MMP). In these cases, CO_2 exists as a gas in the reservoir, creating a scenario of an immiscible gas flood.

Permeability is one of the major factors affecting flow of fluids in the reservoir. It indicates the ability of a rock to transmit fluid. When two or more fluids exist in the reservoir, we have what is known as the relative permeability. This enables a rock to transmit a particular fluid, in the presence of the other fluids. Thus, permeability values are a major factor for the recovery of oil from a reservoir.

Capillary pressures are the other important factors that give the difference in pressures across the interface of two immiscible fluids. Oil and water are an immiscible pair of fluids. Therefore capillary pressures most definitely exist between the interfaces of these two fluids. Low-salinity water, seawater and formation water are considered a single phase, since waters with varying salinities do mix.

Oil and CO_2 are a miscible pair at high pressure and temperature conditions. This is because CO_2 dissolves in oil, and multiple components of oil dissolve back in CO_2. This transfer process carries on until a fluid with uniform concentration is achieved. This essentially means both the fluids are miscible. However, this transfer process is not well defined. It takes place over a varied period of time in the reservoir. Factoring in formation water yields a three-phase system – oil-water-CO_2, or a two-phase system, such as an oil - CO_2 rich phase and water, depending on the local conditions in the reservoir. The presence of a CO_2 flood below the MMP in the

reservoir, automatically generates a three-phase scenario, because oil and CO_2 are not miscible below MMP conditions. Therefore, a corresponding three-phase relative permeability model is used (Stone 1973).

When dealing with formation water floods, low-salinity water floods, or seawater floods, a two-phase flow scenario exists in the reservoir. Hence, a two-phase relative permeability curve is important in this case. When dealing with CO_2 floods, again a two-phase or a three-phase flow exists in the reservoir. Thus a representative two-phase or three-phase relative permeability curve is used for fluid flow calculation. These relative permeability values change based on various local conditions in the reservoir, which are functions of the pressures, temperatures and various fluid saturations with time.

Optimizing the variables involved in waterflooding, such as salinity, CO_2 concentration, and permeability, can increase productivity in secondary and tertiary oil recovery processes.

1.1 Low-Salinity Waterflooding in Sandstones

Lowering the salinity of water being injected can improve recovery of oil in sandstone reservoirs as observed by Lager et al. (2006), Webb et al. (2004) and Seccombe et al. (2008). McGuire et al. (2005), Seccombe et al. (2008), Lager et al. (2008), Skrettingland et al. (2011) observed results in waterflooding efficiency varying from 2 to 40 %, and in improved oil recovery from 6 to 12 % from LSW in coreflooding experiments. Numerous mechanisms of oil recovery by LSW have been stated in literature. Tang and Morrow (1999) reported the requirement of connate water and polar

crude oil components for noticing IOR during LSW. Subsequently Lager et al. (2006) stressed the importance of the presence of divalent cations in the formation water as a main requirement for ion exchange to take place with injected LSW. Skauge et al. (1999) showed that acidic and basic components play a dominant role in wettability alteration. Somasundaran (1975) mentioned that the quartz surfaces were more sensitive to the basic components present in the crude oil. Tweheyo et al (1999) showed wettability alteration for sandstone core plugs from two oil fields in North Sea upon addition of acidic and basic components to a mineral oil. Farooq (2010) found that for surfaces that adsorbed high TAN (Total Acid Number) crude oil, the high-salinity waters did not alter the wettability. But for the same case, low salinity waters altered the wettability from a neutral to a more water wet scenario. When Farooq (2010) tested a low TAN crude oil, the high-salinity waters changed the wettability from a neutral to a more water wet scenario, and the low salinity waters did not show any further improvement when compared to the high TAN crude oil case. Nanji et al. (2012) tested the effects of various polar components of a crude oil on its recovery by high and low salinity waterflooding. They observed a decrease in pH of reservoir brines with an increase in surrounding temperatures. They found out that the oils which had asphaltenes and acidic components extracted showed a water wet character for Berea sandstones, whereas the oils with reduced basic components showed oil wet or intermediate wet characteristics.

An incremental oil was recovered by low salinity was associated with two things: the initial wetting conditions, and internal fines migration of particles. When crude oil

was deprived of acidic or basic components, release of fines needed a very low salinity water (890 ppm), but in systems which had a similar acid/base interaction, fines migration occurred at a relatively higher salinity (3,813 ppm). In general, the presence of acidic components (higher TAN/TBN (Total Base Number) ratio) seemed to be a more favorable environment for low salinity waterflooding. Seccombe et al. (2008) showed that the clay content in the reservoir was directly proportional to the improved oil recovery by LSW, as clays cause potential fines migration which leads to increased contact with smaller pores in the reservoir.

Lager et al. (2006) proposed the theory of EDL (Electric Double Layer) expansion and RezaeiDoust et al. (2010) discussed the MIE (Multiple Ion Exchange) theory, during low salinity waterflooding. The EDL theory states a first Stern layer closest to the clay surface, held by vander waals forces connecting the divalent cations to the negatively charged clay minerals, followed by a second diffuse layer composed of free ions with opposite polarities. The Stern layer is strong to any thermal motion, and thus holds the divalent ions, making them immobile. The diffuse layer strongly depends on the level of ionic strength, and varies depending on thermal motion. Lingthelm et al. (2009) added to the theory of EDL that, clay minerals released from the pore walls are negatively charged and act as colloid particles. The divalent cations, Ca^{2+} and Mg^{2+} present in the connate water, act as bridging media to the negative portions of clay minerals and oil. This bridging involves chemical bonds formed between divalent ions and clay minerals, resulting in organometallic complexes suspected to be the major factor of oil retention in the rock. A decline in the level of free divalent cations in

injected waters triggers a reduction in the ionic strength of the diffuse layer, thus causing an expansion in this layer. Following this, electrostatic repulsion forces cause the removal of chemical bonds between the divalent ions, rock, and oil components, thus releasing those of oil and rock. This can cause potential fines migration. The EDL is said to expand upto 5,000 ppm TDS (Total Dissolved Solids) of surrounding aqueous medium. The MIE theory states that the influx of low salinity water with Na^+ cations is said to trigger ion exchange while there is an expansion in the diffuse layer, removing any organo metallic complexes and polar organic compounds from the clay surfaces, and replacing them with free Na^+ cations

LSW has been observed to have similar mechanisms to that of alkaline waterflooding relating improved recovery to an increased pH environment, according to McGuire et al. (2005). Increase in pH and the alkaline flooding behavior is said to result in decreased interfacial tension and emulsification of oil into water as mentioned by Callegaro et al. (2013). Improved oil recovery during LSW without an increase in surrounding pH has also been observed by Austad et al. (2010). Although several mechanisms and criteria have been mentioned, IOR has not been obtained in many cases that meet the criteria for LSW according to Skrettingland et al. (2010). Researchers in BP, Lager et al. (2007), have experimentally observed effluents' pH increase by 1 to 3 units, production of fines, and increase at pressure at the end of the flooded core indicating a decrease in permeability due to fines migration or oil/water emulsions. Fjelde et al. (2012) stated that there was a definite interaction between rock and brines during LSW based on analyses of effluent samples for pH and cations. They asserted

that LSW potential must be considered in a case by case basis depending on interactions between formation brine present in the reservoir, low salinity brines being injected, components of oil in the reservoir and the nature of the rock.

1.2 Wettability Alteration during Low-Salinity Waterflooding

Previous research has established that low-salinity water injection generally alters the wettability of the rock to a more water-wet state. However, Fjelde et al. (2012) observed that when diluted formation water was used as the injected low-salinity brine, the wettability in sandstone cores with high clay content was altered to a less water-wet state, enabling oil production over a longer period of time.

1.3 Low-Salinity Water-Alternating-CO_2 Flooding

CO_2 flooding is the leading EOR process in light oil and medium oil reservoirs (Ghedan 2009; Alvarado et al. 2010). Ghedan (2009) reviewed that miscible and immiscible continuous CO_2 injection, carbonated waterflooding, and the huff and puff process are the most commonly used EOR techniques in the field. Teklu et al. (2014) stated that the injection of CO_2 altered wettability of carbonates and sandstones toward a more hydrophilic condition.

Al-Mutairi et al. (2014) performed wettability measurements at reservoir temperatures and immiscible CO_2 pressures on carbonate cores, and showed that exposing oil-wet carbonates to brine-saturated CO_2 causes wettability alteration to an

intermediate-wet state. The magnitude of wettability alteration is directly proportional to the CO_2 concentration in brine.

Bennion et al. (2008) performed experiments concluding that increment in CO_2 solubility with low-salinity brine results in CO_2-brine IFT (Inter-facial Tension) reduction. Teklu et al. (2014) stated that this in turn could cause wettability alteration due to a decrease in IFT between the CO_2-brine phase and the oil phase.

1.4 Simulation Studies and SCAL Properties

SCAL experiments to determine relative permeability curves and capillary pressures are more expensive and time consuming when compared to Conventional core analyses, which measure just the porosities and permeabilities of a core. Keeping this in mind, there are several mathematical models used industry wide to generate SCAL properties in advance of time. These include Prediction models, Network models and Empirical models. Prediction models have their own assumptions and rely purely on theory, thus making them unreliable for a wide variety of cases. Network models are very core plug specific. Empirical models are the most widely used by the industry, and those which have a theoretical backing are more reliable.

Fjelde et al. (2012) estimated Kr and Pc curves for unsteady-state waterflooding experimental cases performed with the help of the Sendra™ simulator, and they observed that the nature of the curves were more water wet for formation waterflooding scenarios when compared to the case of LSW with diluted formation water. While using Eclipse™ to model LSW scenarios, Callegaro et al. (2013) added transmissibility

multipliers during low-salinity water injection to model the permeability reduction. The Pc curves were considered negligible in their 1-D simulation cases.

Mohamad et al. (2000) generated several oil-water and gas-oil relative permeability correlations using a two-phase linear regression technique based on published relative permeability experimental data over a wide variety of sandstone and carbonate cores, from published literature and industry sources. They observed that the correlations proved to be more effective in matching experimental data than compared to other existing industry standard correlations, for conventional waterflooding and gasflooding techniques.

Odeh (1959) performed experiments to investigate the effects of viscosity ratio on the relative permeability of the nonwetting phase, Kro, and found maximum differences in relative permeability values due to viscosity ratios of nonwetting phase to wetting phase, occurring at points of minimum brine saturation.

Johnson et al. (1957) developed a method to experimentally calculate individual relative permeability curves from data collected during a displacement test, based on strong theoretical assumptions. These theories state the flow velocity to be high enough to achieve a stabilized displacement scenario. The resulting pressure drops across the core are very high compared to the capillary pressures between the phases. This forces the portion of the core where capillary pressures are dominant to be a negligible level fraction as compared to the total pore space.

Jerauld et al. (2008) investigated the capabilities to model low salinity waterflooding, and observed that the nature of relative permeability curves used to match

experimental tests display a characteristic behavior found in many floods of more favorable fractional-flow behavior and a similarity in water relative permeabilities at high- and low-salinity residual-oil saturations, as shown in **Figure 1**.

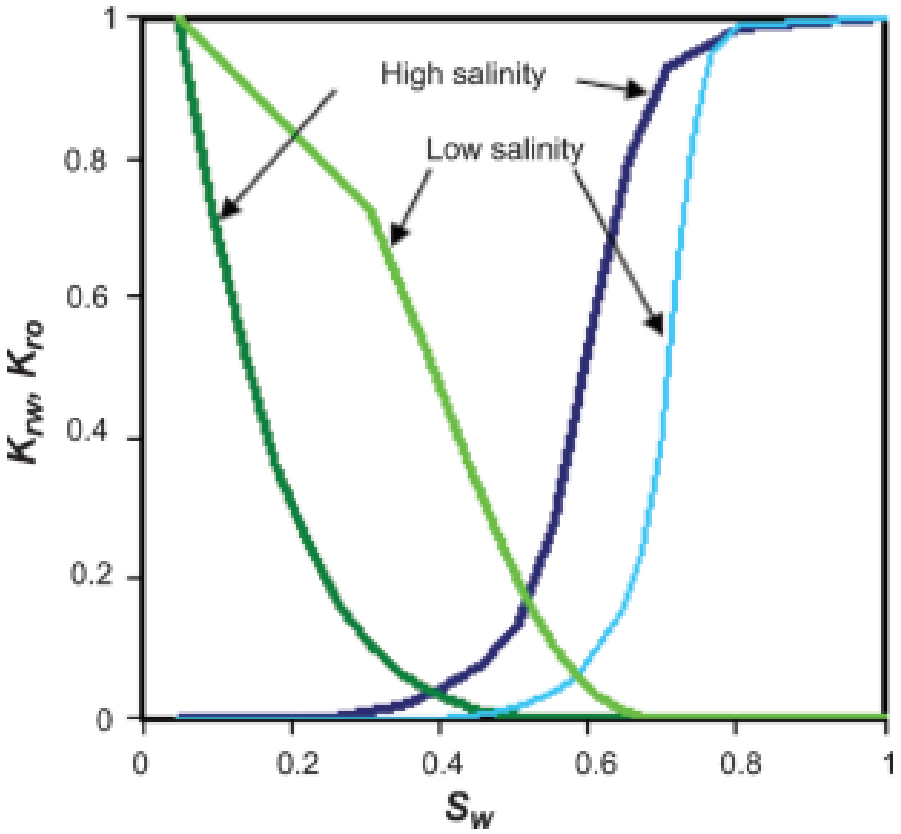

Figure 1—High- and low-salinity relative permeability curves used in the simulations by Jerauld et al. (2006).

All the studies performed so far in LSW have been confined to high permeability sandstone reservoirs and light oils. There has been no detailed study which verifies stated theories in LSW from the perspective of low-permeability sandstone reservoirs and medium oils. This work highlights some interesting facts that were observed with

respect to LSW performance in the above stated scenarios. In the following sections, firstly, the apparatus and procedures of the experiments conducted have been mentioned in the Experimental Materials' and Experimental Studies' sections followed by a description of the tools and features of the simulation software package used for interpretation of experimental results. Next, the Results and Discussions section will help the reader understand the physics involved to explain experimental results with the help of simulation models. Lastly, the Conclusions of this study have been stated, and the capability of extending the current work to a more broader scope has been laid out under Future Work And Recommendations.

2. EXPERIMENTAL MATERIALS

2.1 Cores

Seven cylindrical cores of 1.5 in. diameter and 3 in length were cut from Grey Bandera sandstone outcrop rocks with a core bit. To ensure a consistent permeability anisotropy range, the cores were drilled in a single direction. **Table 1** reports the petrophysical properties of each core sample.

Core ID	HK-1	HK-2	HK-3	HK-5	HK-6	HK-7	HK-8
Length (in.)	2.96	2.90	2.86	2.85	2.85	2.91	2.95
Porosity (vol%)	19.07	18.69	18.56	18.65	18.76	18.87	18.90
Absolute permeability (md)	6.38	6.54	6.11	5.91	6.17	6.35	6.13
Connate water saturation (%)	38	35	29	41	**32**	48	39
Initial oil saturation (%)	62	65	71	59	68	52	61

Table 1—Petrophysical properties of the Grey Bandera sandstone cores.

Rectangular core tile substrates of the dimensions 0.62 in. x 0.72 in. x 0.25 in. cut from a Grey Bandera sandstone core plug were used in measuring contact angle.

2.2 Fluids

2.2.1 Brines

Five different brines were used in this study, namely: formation water, seawater, 0.5 wt% NaCl solution, 0.5 wt% KCl solution, and 0.5 wt% $MgCl_2$ solution. All brines were prepared by mixing reagent-grade salts with deionized water. **Table 2** lists the compositions of the synthetic brines.

Salt	Formation Brine, mg/l	Seawater Brine, mg/l	Low-salinity Brine, mg/l	Low-salinity Brine, mg/l	Low-salinity Brine, mg/l
NaCl	137,735	38,386	5,000	-	-
$CaCl_2.2H_2O$	38,881	2,435	-	-	-
$MgCl_2.6H_2O$	13,463	19,058	-	5,000	-
Na_2SO_4	547	5,263	-	-	-
$NaHCO_3$	242	265	-	-	-
KCl	-	-	-	-	5,000
Total dissolved solids , (TDS)	174,156	54,680	5,000	5,000	5,000

Table 2—Composition of synthetic brines.

Their viscosities and densities at reservoir temperature and atmospheric pressures appear in **Table 3**.

Brine	Density, g/cm^3	Viscosity, cp
Formation Brine (TDS = 174,156 ppm)	1.1145	0.626
Seawater Brine (TDS = 54,680 ppm)	1.0204	0.496
Low-salinity Brine (TDS = 5,000 ppm)	0.9871	0.439

Table 3—Density and viscosity of prepared brines at 149°F and 14.7 psi.

The DMA 4100 densitimeter was used to measure the density of the brines, whereas a capillary viscometer was used to measure the viscosity. The initial connate water present in the cores was formation water which consisted of divalent Ca^{2+} and Mg^{2+} cations.

2.2.2 Crude Oil

A medium dead crude oil sample from west Texas was centrifuged at 5,000 rpm for five minutes to remove any suspended solids and to separate it from the aqueous phase. Following this, it was filtrated through a sandstone core to minimize future solids plugging or emulsion problems. **Table 4** lists the properties of the crude oil used, and **Table 5** gives the crude oil composition. The density and viscosity of the crude oil were measured at 149°F and atmospheric pressures.

Crude Oil	°API	Temperature, °F	Density, g/cm^3	Viscosity, cp
West Texas Crude Oil	29	74	0.8716	19.56
		149	0.8023	5.25

Table 4—Properties of crude oil at 14.7 psi.

No.	Component	Concentration, wt %
1)	Benzene, 1,3-dimethyl-	10.54
2)	Octane, 2,6-dimethyl-	7.05
3)	Benzene, 1,2,4-trimethyl-	13.63
4)	Benzene, 1-ethyl-2,3-dimethyl-	8.04
5)	Benzene, 1,2,4,5- tetramethyl-	5.39
6)	Dodecane	4.21
7)	Dodecane, 2,6,10-trimethyl-	5.93
8)	Tetradecane	2.66
9)	Dodecane, 2,6,11-trimethyl-	4.00
10)	Pentadecane	4.07
11)	Hexadecane	3.93
12)	Pentadecane, 2,6,10,14-tetramethyl-	6.18
13)	Hexadecane, 2,10,10-trimethyl-	5.35
14)	Hexadecane, 2,6,10,14-tetramethyl-	6.18
15)	Nonadecane	2.13
16)	Eicosane	2.96
17)	Heneicosane	2.37
18)	Docosane	1.86
19)	Tricosane	1.58
20)	Tetracosane	1.96

Table 5—Composition of west Texas crude oil.

3. EXPERIMENTAL STUDIES

3.1 Rock Characterization

The Grey Bandera sandstone rock was characterized using XRD. The XRD (X-Ray Diffraction) test results were analyzed for the mineralogy composition of the rock, as given in **Table 6**. These rocks were significant sources of clay minerals.

Mineral	Concentration, wt%
Quartz	80
Kaolinite	7
Illite	11
Dolomite	2

Table 6—Mineralogy of Grey Bandera sandstone cores from XRD analysis.

The pore size distribution of the Grey Bandera core was measured by Core Labs, with the maximum and average pore-throat radii being 6.61 μm and 1.81 μm.

3.2 Interfacial Tension Measurements

3.2.1 Setup

The IFT measurements were performed using the Drop Shape Analysis (DSA) equipment, shown in **Figure 2**. The DSA was comprised of the following components:

1. An HP/HT (High Pressure/ High Temperature) view chamber cell (Eurotechnica GmbH, Germany, P_{max} = 10,000 psi, T_{max} = 392°F, stainless steel material 1.4436).
2. A capillary needle located within the HP/HT chamber for injecting crude oil droplets.
3. An oil accumulator with stored crude oil, connected to the capillary needle, and an ISCO syringe pump to aid in injection at set pressure / rate.
4. A temperature controller (Hillesheim HT 40, Germany, control range: 32-212°F) to control inner temperature of HP/HT chamber.
5. A K-type thermocouple with an accuracy of 0.1°K, located inside the HP/HT chamber to monitor temperature.
6. A compressed N_2 / CO_2 cylinder for applying pressure in the HP/HT chamber
7. A pressure transducer to monitor HP/HT chamber pressure.
8. An image data acquisition system to acquire high definition images of crude oil droplet.
9. The DSA software for crude oil droplet image analysis.
10. A white light source to illuminate HP/HT chamber.
11. An inlet valve to inject brine inside HP/HT chamber.

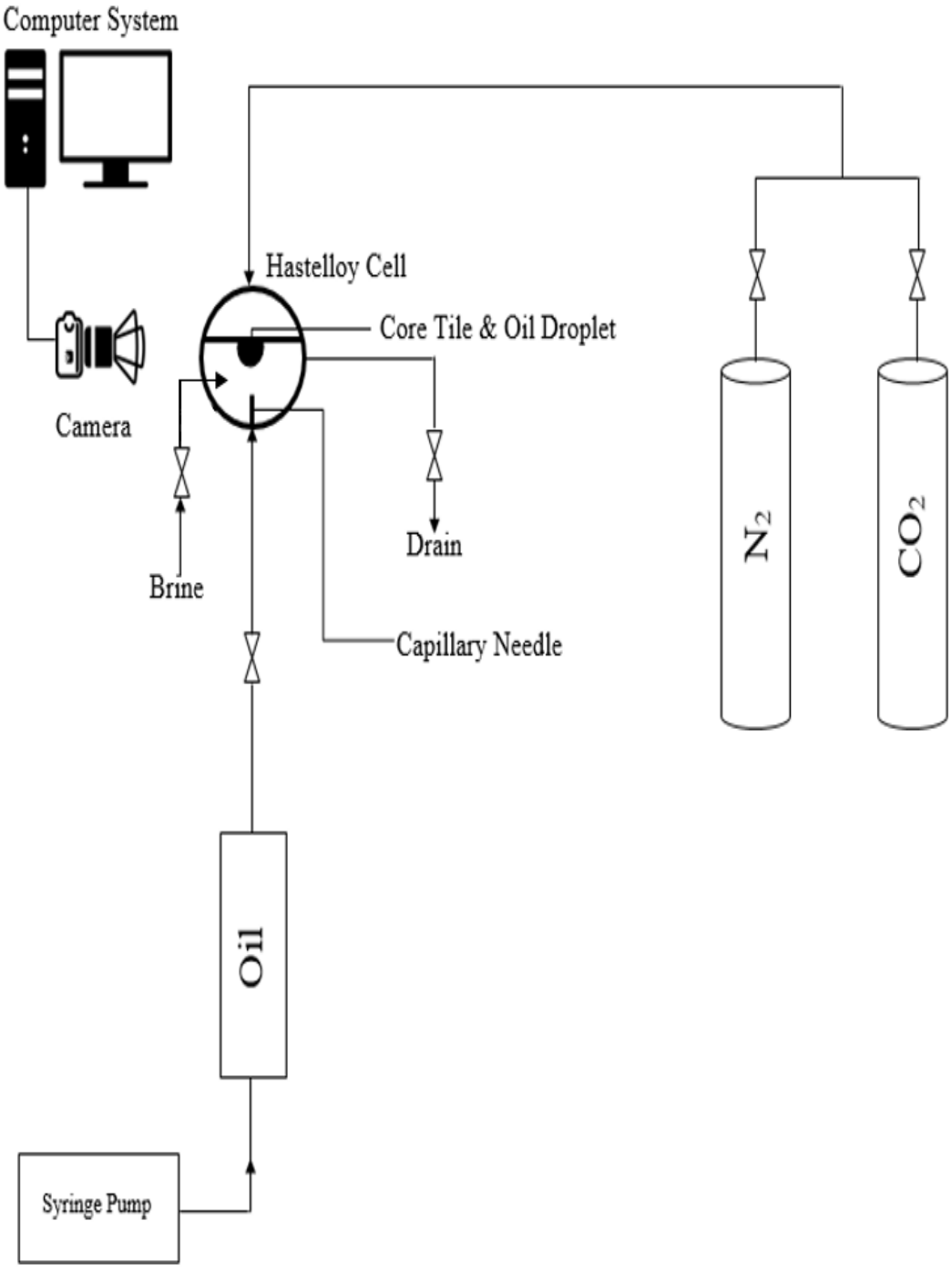

Figure 2—A schematic diagram of the drop shape analyzer.

3.2.2 Procedure

The experiments were performed as follows*:*

1. HP/HT chamber was cleaned with acetone followed by DI water, and dried.
2. The HP/HT chamber was tightly sealed, and the specific brine of study was injected into the chamber, filling it to its maximum storage capacity.
3. The temperature of HP/HT chamber was set using the temperature controller.
4. Pressure was applied by injecting compressed N_2/CO_2 into the HP/HT chamber. Depending on the temperature or pressure conditions within the chamber, pressurizing gas may or may not be soluble in brine.
5. A light source and camera were adjusted to obtain a clear imaging view on DSA software.
6. An oil droplet was injected through the capillary needle using the ISCO syringe pump, at a constant pressure set higher than that of the chamber pressure, to obtain a pre-decided drop volume, and the injection valve was tightened to close, in order to hold the drop at the needle tip, as viewed in the DSA software.
7. One hour was given to attain oil droplet - brine stability at pre-set HP/HT chamber conditions.
8. The DSA software with in built correlations was used to analyze oil droplet shape to determine oil - brine IFT.

3.3 Contact Angle Measurements

3.3.1 Setup

The DSA equipment, as described in the IFT Measurements section, with schematic, as in Figure 2, was used. The additional components for measuring contact angles were:

1. A core tile substrate holder.
2. Bandera grey core tile substrates.

3.3.2 Preparation for Contact Angle Experiments

For all the experiments, a rectangular core tile was used as the rock substrate, and it was prepared using the following procedure:

1. The rectangular tile core substrates were polished on both lateral faces using sandpaper of sizes 400 - mesh and 200 - mesh to minimize the contact angle hysteresis caused by surface roughness.
2. After polishing, the substrates were immersed in formation brine for 24 hours and then vacuumed for 6 hours.
3. The substrates were then placed in crude oil and centrifuged at 3,000 rpm for 60 minutes to attain connate water saturation, Swc, in the substrates.
4. Finally the substrates were aged by immersing them in crude oil at a reservoir temperature of 149°F for a period of two weeks.

3.3.3 Procedure

The procedures were similar to those of the interfacial tension experiments, the only difference being that a prepared core tile substrate was placed in a tile holder, which was fixed in the HP/HT chamber, ensuring the tile surface to be horizontally oriented above the capillary needle, before filling it with the surrounding brine and setting the chamber at reservoir temperature and pressure. After this, an oil droplet was injected at a higher pressure than that of the chamber, and released via the capillary needle onto the surface of the core tile substrate. The DSA software was then used to analyze the oil droplet to determine the contact angle.

3.4 Corefloods

3.4.1 Setup

Figure 3 presents the schematic diagram of the coreflood apparatus. The components of this setup are listed as follows:

1. A three in. vertically mounted stainless steel core holder, with a rubber sleeve within for applying overburden pressure on the core.
2. Three accumulators for storing oil, CO_2 and brine.
3. An ISCO Syringe pump used for injecting fluids into the core at specified rates or pressures.
4. A pressure transducer to monitor pressure drop across the core.
5. A N_2 cylinder for applying overburden pressure on core and back pressure at core outlet.

6. A hydraulic oil pump to inject hydraulic oil into a cavity between the internal surface of the core holder and the rubber sleeve, for balancing applied overburden pressure on core.
7. A CO_2 cylinder for injecting gas phase CO_2 into the core.
8. A LABVIEW^{TM} software to record pressure drop measured by the pressure transducer with time.
9. A heating oven containing the core holder, to perform experiments at reservoir temperatures.

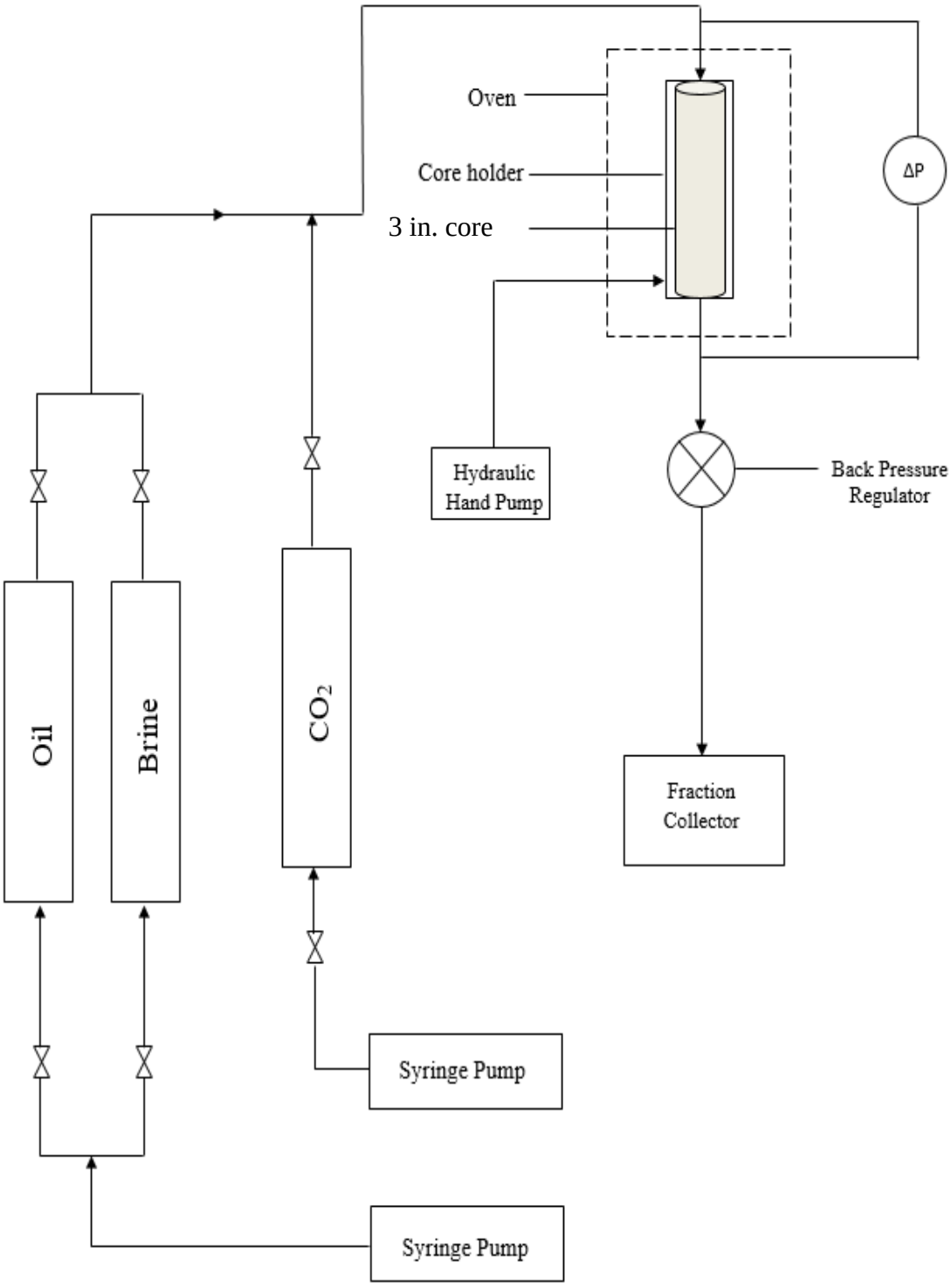

Figure 3—A schematic diagram of the coreflood apparatus.

3.4.2 Preparation of Cores

Following were the procedures. A summary of the core preparation experiments listing initial core properties appears in Table 1:

1. Seven 3 in. Grey Bandera cores were dried in an oven at 250°F for a period of 48 hours, and weighed. s

2. The cores, namely HK-1, HK-2, HK-3, HK-5, HK-6, HK-7 and HK-8, were saturated with synthetic formation brine in a saturation cell for 10 days to achieve ionic equilibrium between the surface of the rock and formation brine.

3. Absolute permeability measurements were conducted on these seven cores by flooding formation brine at low constant rates of 0.5, 1 and 2 cm^3/min, ensuring 100% brine saturation, and then the permeability was calculated using Darcy's law at the stabilized pressures for each rate. The experiments were conducted at room temperature, with an overburden pressure of 1600 psi and a back pressure at core outlet of 500 psi.

4. Pore volume and porosity values were calculated via material balance.

5. Primary drainage experiments were performed on cores HK-1 to HK-8 by flooding them with crude oil at low constant rates of 0.1, 0.2, 0.5 and 1 cm^3/min to establish irreducible water saturation. Pressure and temperature control parameters were similar to those of the absolute permeability experiments. The irreducible water saturations were assumed to be the connate water saturations of the cores.

6. All cores were aged for 14 days by being immersed in crude oil in a sealed steel cylinder and continuously heated in an oven at 149°F. Atmospheric pressure was maintained for this purpose.

4. SIMULATION STUDIES

4.1 Commercial Simulators

The secondary low-salinity waterflooding experiments were investigated using the Eclipse™ Black Oil Reservoir Simulator (2014.1) (E100). Calsep's PVTSim (1.1.23 2016) fluid model package was used to create the black oil fluid model for E100 simulator, based on the oil components and physically measured properties of the crude oil and brines. E100 treats oil, water and gas as three separate phases/components, and uses the individual fluid physical properties and rock properties to perform material balance calculations. The Eclipse™ Compositional Reservoir Simulator (E300) analyzes the material balance calculations by taking individual components of the crude oil into account. In terms of accuracy, the E300 is much more efficient than E100. However, the calculations involved in E300 are complex due to a lot more variables involved, and thus the simulation cases take a longer time to reach completion. The E100 is more versatile in its features, and can model a wide variety of EOR processes. Thus an E100 model calibrated with that of an E300 model would be ideal in modeling complex EOR processes, to save runtime and maintain accuracy. During each waterflood experiment, the injection water salinity and salt type was maintained constant throughout the flood, with connate water saturation being present in the cores. Mixing of injected and connate water brines has been neglected in this study.

4.2 Fluid Model

The PVTSim fluid package proved an efficient tool to model the fluids involved in the experiments. The crude oil sample was modeled by inputting the composition along with the fluid characterization experiments. The use of this package in creating a black oil model provided a calibrated fluid system to that of a compositional fluid model, thus ensuring accuracy in the results. The black oil fluid was modeled by using Equation of States to tune the simulated fluid results with that of the experiments. Crude oil physical property experiments used in matching were viscosity measurements with varying temperatures, and density measurements with varying temperature, both performed at atmospheric pressures. The constant mass expansion and viscosity experiment options were used in PVTSim to input the experimentally measured properties. EOS used for matching density experiments was Peng Robinson 78 Peneloux. The Corresponding States Principal Viscosity / Thermal Condition EOS was used to match the viscosity experiments. **Figure 4** and **5** show the experimental and simulated matches.

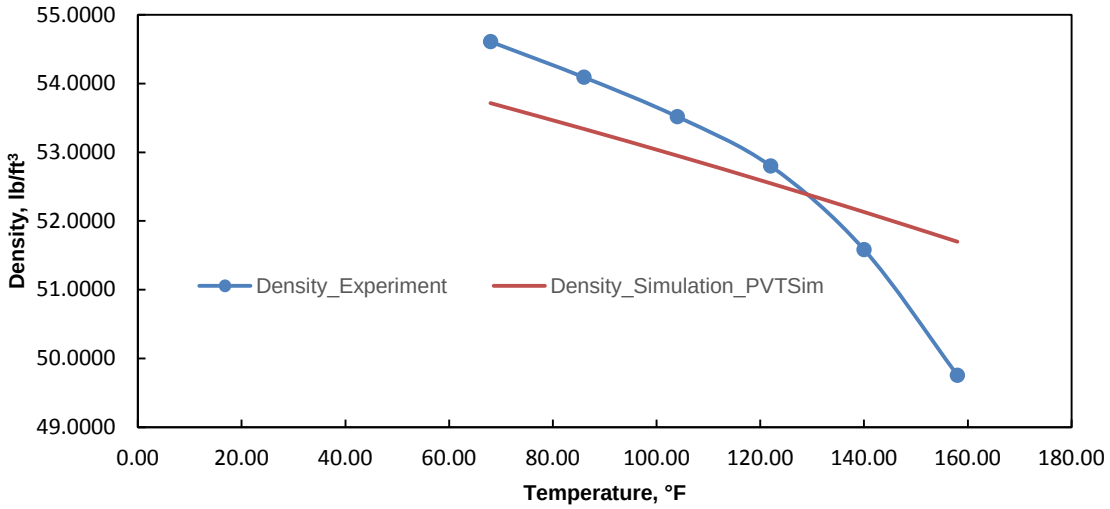

Figure 4—Density vs. temperature - experiment and PVTSim fluid tuning.

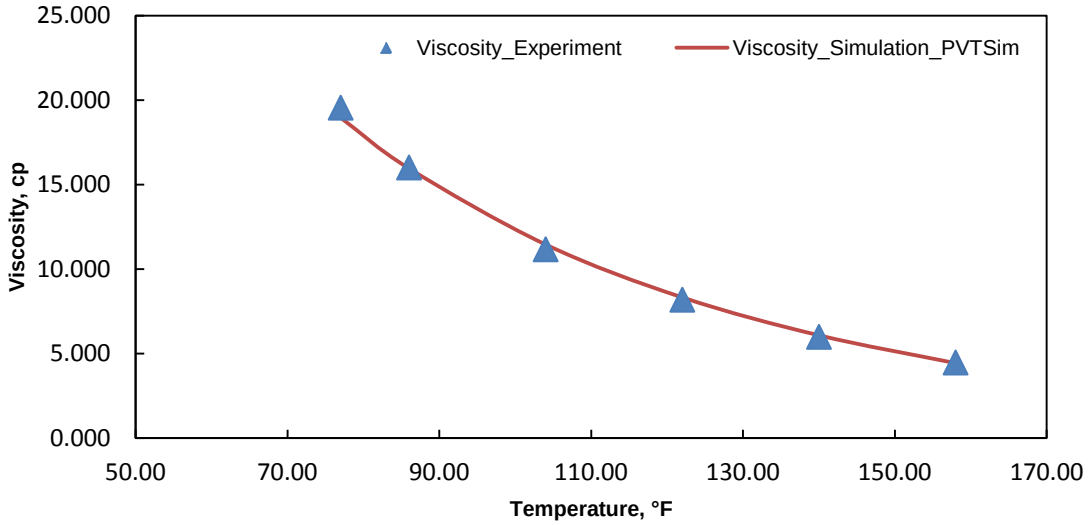

Figure 5—Viscosity vs. temperature - experiment and PVTSim fluid tuning.

4.3 Core Model and Orientation

A radial grid 2-D model was created in E100, using 25 cells along the radial direction, 1 cell in the angular direction and 100 cells along the vertical direction. The cell numbering in E100 is (radial, angular, vertical). The cylindrical model was vertically oriented, similar to the coreflood experiments. The injector was completed in the bottom face at cell (1,1,100), and producer was completed at the top face in cell (1,1,1) **(Figure 6).**

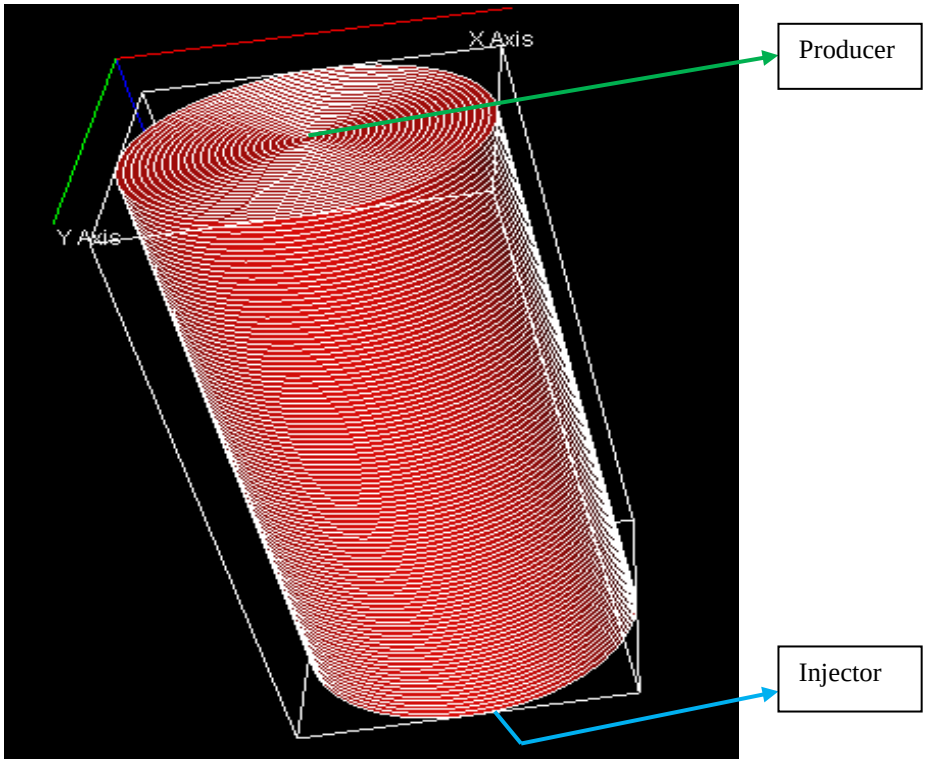

Figure 6—Radial grid simulation model - EclipseTM (2014.1) 100.

4.4 Boundary Conditions

No flow zones were established at all the boundaries, other than the cell boundaries in which the wells have been completed. This ensured that the fluid flow was contained within the core model to prevent any leak via boundary cells, and depicted the net flow of fluids from the injector to the producer, similar to the experiments performed.

4.5 Inputs

The rock porosities and isotropic permeabilities are used for the core model properties. The fluid properties of the crude oil and brines are created from the fluid model in PVTSim, and used as an input to E100. The model is initialized by enumeration, with pressures in all cells being set at the experimental back pressures, and the connate water saturations and initial oil saturations uniformly set across the model. Since this study used homogenous cores, the initial saturation and porosity profiles were uniform along the lengths of the core model. At start, the correlation based relative permeability curves as described under Section 4.6, were used as inputs.

4.6 SCAL Properties

The oil-water relative permeability curves were the main sensitivity parameters, that were created based on correlations for the different brine-oil systems. Capillary pressure curves were considered negligible in this core scale study. The relative

permeability correlations used to create the curves were generated using correlations by Mohamad et al. (2000). Based on the experimental measured properties of our Grey Bandera cores, the correlations used to create oil-water relative permeability curves are given by Equations 1, 2 and 3.

Oil - Water System for Water Wet Sandstones, by Mohamad et al. (2000):

Equation 1:

$$Krow^* = \quad 1 - 3.090996\, Sw^* + 2.8670229\, Sw^{*1.6} - 0.768952\, Sw^{*2}$$

Equation 2:

$$\begin{aligned} Krw^* = \quad & 0.22120304\, Sw^{*1.6} + 0.24933592\, Sorw^2 \frac{Sw^{*3}}{\Phi} \\ & + 21.370925\, Sw^{*2} Sorw^5 + \ 83.491972 \Phi^4 Sw^{*5} Sorw^{1.5} \\ & - 0.4562939\, Swc^3 Sw^{*4} + 1161.07198\, (\Phi^2 Swc\ Sorw\ Sw^*)^2 \\ & - 8.7866012 Sorw^3 Sw^{*2.3} \\ & + \ 0.00000578\, Sw^{*3} \big(Swc\ ln(kbase)\big)^{10} (1 - Sorw)^{0.4} \\ & - \ 12.841061\, Sw^{*2} (ln(kbase)\ Swc)^3 \Phi^6 \end{aligned}$$

Equation 3:

$$\mathrm{Sw}^* = \quad \frac{(\mathrm{Sw} - \mathrm{Swirr})}{(1 - \mathrm{Swirr} - \mathrm{Sorw})}$$

where, Krow = normalized relative permeability to water*

Kro = normalized relative permeability to oil*

Swc = connate water saturation

Krw = relative permeability to water

Kro = relative permeability to oil

Sw = normalized water saturation*

Sorw = residual oil saturation

φ = porosity

kbase = base permeability

Kro = normalized relative permeability to oil*

The oil-water curves in all conducted waterflooding experiments of this study fell under the general water wet category, based on the conditions specified by Mohamad et al. (2000). The values of input variables as stated in the above equations were available from the experiments. The base permeability was chosen as Keo at Swirr for all the waterflooding experiments, as required by the correlations. The oil - water relative permeability curves were generated from the correlations for three different experiments, namely formation water - crude oil system from C-1, seawater - crude oil system from C-2, and low salinity 5,000 ppm NaCl solution - crude oil system from C-5.

4.7 Outputs

Each core flood experiment was simulated using the respective inputs as described above. The results plotted were the Cumulative Oil Recovery Factor and the Pressure Drop across the core.

5. RESULTS AND DISCUSSION

5.1 Experimental Studies

5.1.1 Interfacial Tension Measurements

Six water samples were tested with the west Texas crude oil droplet, separately using N_2 and CO_2 as HP/HT chamber pressurizing mediums. All experiments were performed to measure IFT values with respect to time, at five minute intervals for a total period of seven hours. **Table 7.** gives the experimental results.

Experiment ID	Pressurizing Medium	Sample Tested	Average IFT Value, mN / m
I-1	N_2	Formation Brine (174,156 ppm) - Crude Oil	13.96
I-2		Seawater (54,680 ppm) - Crude Oil	10.02
I-3		NaCl Solution (5,000 ppm) - Crude Oil	19.09
I-4		KCl Solution (5,000 ppm) -Crude Oil	19.22

Table 7—Summary of interfacial tension experiments at T = 149°F, P = 500 psi.

Experiment ID	Pressurizing Medium	Sample Tested	Average IFT Value, mN / m
I-5	N_2	$MgCl_2$ Solution (5,000 ppm) - Crude Oil	20.23
I-6		DI Water - Crude Oil	15.75
I-7	CO_2	Formation Brine (174,156 ppm) - Crude Oil	20.16
I-8		Seawater (54,680 ppm) - Crude Oil	16.37
I-9		NaCl Solution (5,000 ppm) - Crude Oil	18.38
I-10		KCl Solution (5,000 ppm) - Crude Oil	18.45
I-11		$MgCl_2$ Solution (5,000 ppm) - Crude Oil	17.44
I-12		DI Water - Crude Oil	17.87

Table 7 Continued

The IFT values ranged between 10.02 and 20.23 mN/m for the tested fluids, and were consistent over the seven-hour period, in an N_2 pressurizing medium. N_2 is a more inert medium as compared to CO_2, and thus will yield a more accurate oil-water IFT value without much influence from the pressurizing gas phase. The values are shown in **Figure 7**. Seawater-crude oil systems resulted in lower IFT values in comparison to that of formation water-crude oil systems, whereas the three different cation low salinity

waters yielded higher IFT values. Among the three low-saline solutions, the IFT values were similar. The theory of low-salinity water systems having lesser interfacial tensions as compared to high-saline systems did not apply in this study. As Vijapurapu and Rao (2004) reported, a critical brine concentration existed which lowered the IFT to a minimum value, and upon further dilution of formation brine, the IFT increased. In this study, seawater with a brine concentration of 54,680 ppm seems to be nearer to the critical brine saturation for the given fluid system.

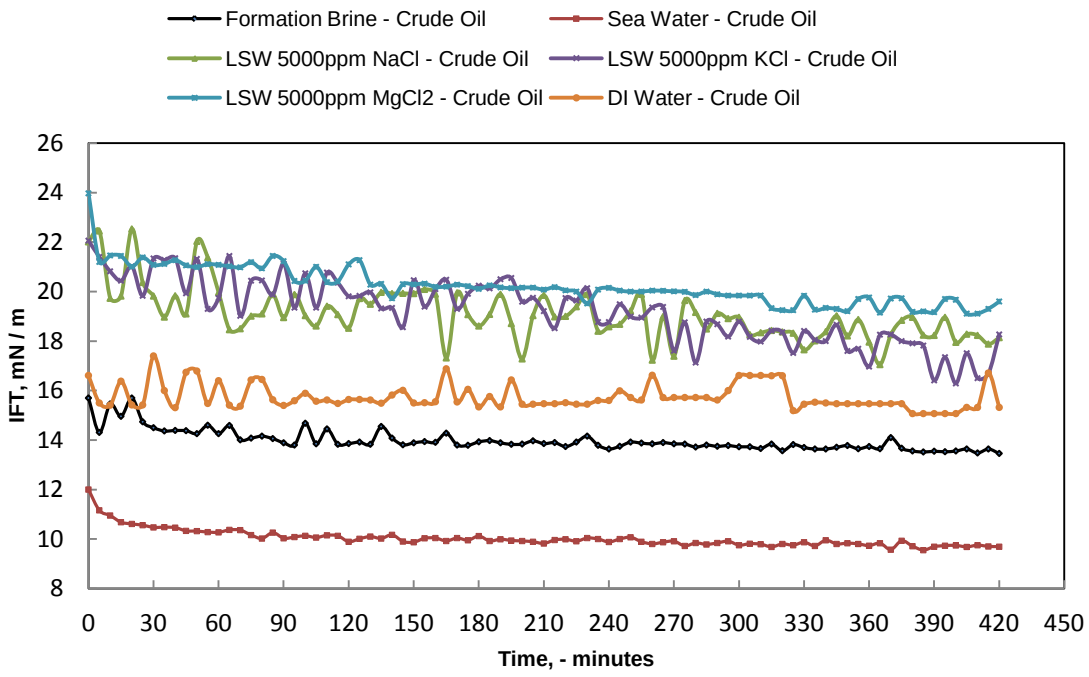

Figure 7—Interfacial tension measurements of fluids with N_2 as pressurizing system, T = 149°F, P = 500 psi.

When CO_2 was used as a pressurizing medium, the IFT values increased for the high saline waters (seawater and formation water)-crude oil systems. But in the case of all low-saline 5,000 ppm water-crude oil systems, the IFT values decreased. This observation of low saline water-crude oil systems having decreased IFT values upon dissolving CO_2 was in accordance with that stated by Teklu et al. (2014). On average, the IFT values in the CO_2 pressurizing systems ranged between 16.37 and 20.16 mN/m, and were consistent over the seven-hour period. The values are shown in **Figure 8.**

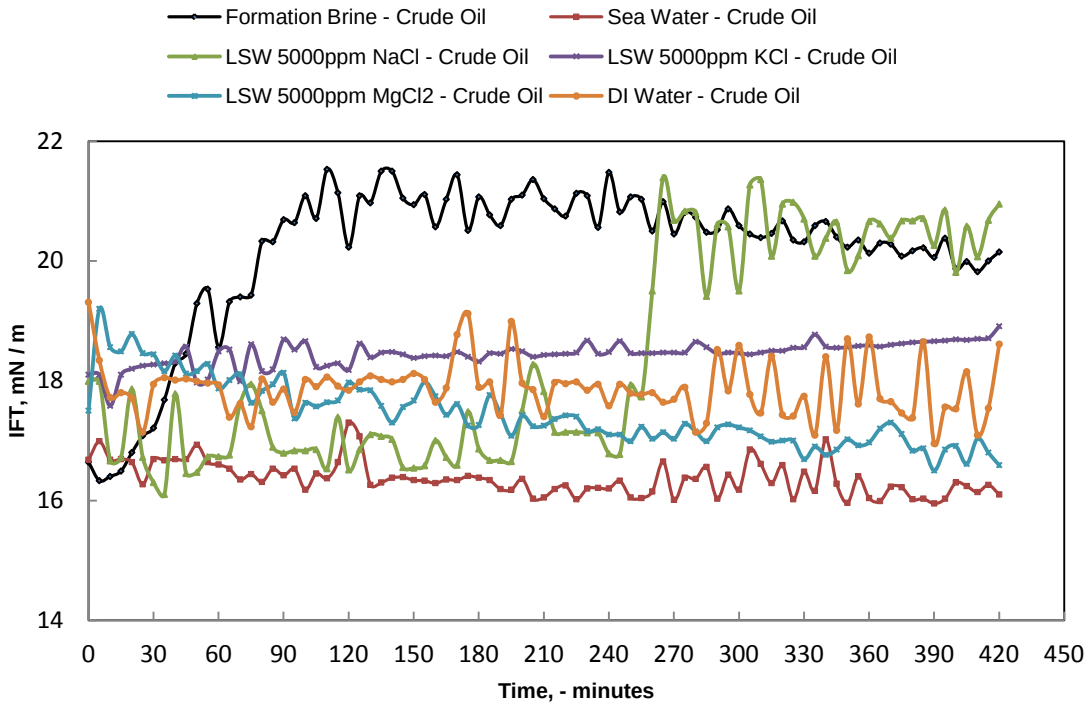

Figure 8—Interfacial tension measurements of fluids with CO_2 as pressurizing system, T = 149°F, P = 500 psi.

5.1.2 Contact Angle Measurements

Five brines were tested with the west Texas crude oil droplet, separately with N_2 and CO_2 pressurizing media. The contact angles were measured at 30 minute intervals for a period of seven hours. The experimental results are tabulated in **Table 8**.

Experiment ID	Pressurizing Medium	Sample Tested	Average Contact Angle Value, °
CA-1	N_2	Formation Brine (174,156 ppm) - Crude Oil	52.63
CA-2		Seawater (54,680 ppm) - Crude Oil	59.72
CA-3		NaCl Solution (5,000 ppm) - Crude Oil	49.09
CA-4		KCl Solution (5,000 ppm) -Crude Oil	46.19
CA-5		$MgCl_2$ Solution (5,000 ppm) - Crude Oil	35.45
CA-6	CO_2	Formation Brine (174,156 ppm) - Crude Oil	69.17

Table 8—Summary of contact angle experiments at T = 149°F, P = 500 psi, on Bandera Grey rock tile substrates.

Experiment ID	Pressurizing Medium	Sample Tested	Average Contact Angle Value, °
CA-7	CO_2	Seawater (54,680 ppm) - Crude Oil	47.54
CA-8		NaCl Solution (5,000 ppm) - Crude Oil	51.11
CA-9		KCl Solution (5,000 ppm) -Crude Oil	38.72
CA-10		$MgCl_2$ Solution (5,000 ppm) - Crude Oil	52.27

Table 8 Continued

The C-A values ranged between 35.45° and 59.72° for the tested fluids, with N_2 as the pressurizing medium, thus proving the rock to be water wet in presence of all the brines. N_2 ensured an inert pressurizing medium to obtain accurate C-A's of the oil/water/rock system. The values were consistent over the seven-hour period. All the low saline waters yielded the most water-wet states in comparison to formation water. 5,000 ppm $MgCl_2$ solution-crude oil system resulted as most water wet, followed by 5,000 ppm KCl and 5,000 ppm NaCl solutions. Seawater-crude oil systems yielded the least water-wet states among all the brines. Seawater consisted of a higher divalent cation concentration (Mg^{2+} and Ca^{2+}combined) than formation water and low salinity brines. These two divalent ions have a tendency to bind with clays and form an organometallic complex with the negatively charged components of the clays and crude

oil, as stated by Lingthelm et al. (2009). Thus this could be the reason for a less water-wet state in the case of seawater. Based on the C-A results of low salinity brines, the earlier stated MIE theory and EDL theory seemed to alter the wettability, yielding a more water-wet state. In the case of 5,000 ppm $MgCl_2$ solution, as explained by the EDL theory, the ionic strength of the divalent Mg^{2+} ions is much lesser than that of the total divalent ions in connate water, thus resulting in the possible expansion of the diffuse layer, and consequent release of oil components. For the cases with monovalent low saline brines, as explained by the MIE theory, a shock in salinity causes an expansion of the electric double layer followed by replacement of divalent ions that are bounded to the clays by that of free monovalent ions from bulk low saline solution. This ion-exchange processes causes a release of the oil particles earlier bound to the rock via organometallic complexes through the divalent ions. **Figure 9** shows the results of contact angle measurements for N_2 pressurizing system.

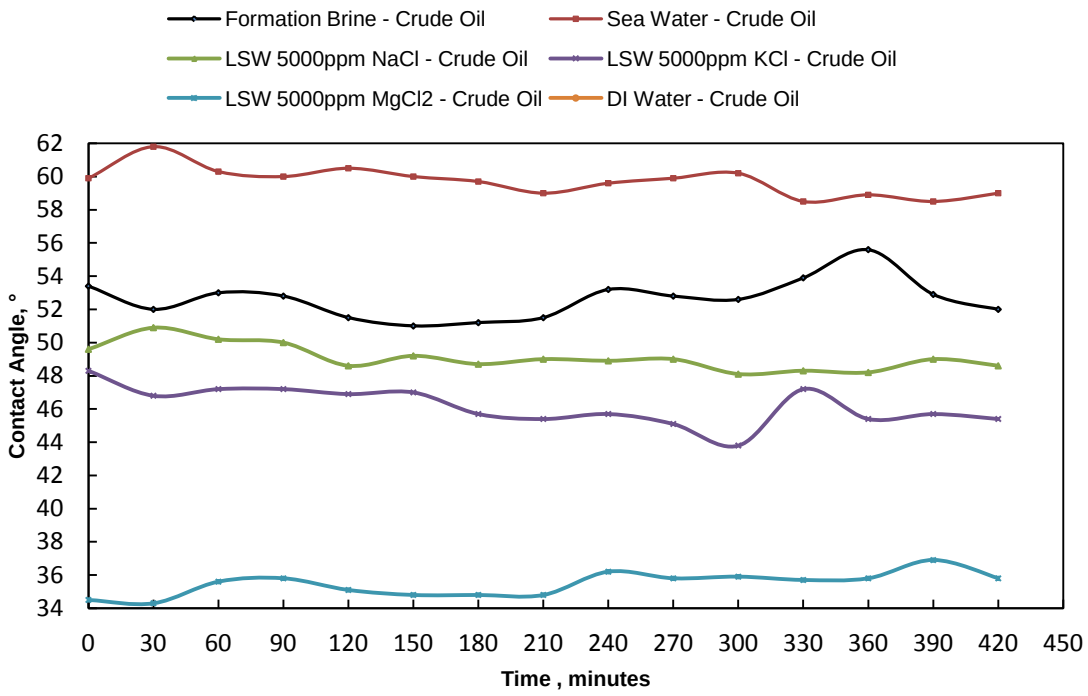

Figure 9—Contact angle measurements of fluids on Grey Bandera rock tile substrates, with N_2 as pressurizing system, T = 149°F, P = 500 psi.

When CO_2 was used as the pressurizing fluid, the values ranged between 38.72° and 69.17°, and were consistent over the seven-hour period. The system with seawater and 5,000 ppm KCl solution showed a decrease in C-A values. The other fluid systems involving formation water, 5,000 ppm $MgCl_2$ solution and 5,000 ppm NaCl solution with crude oil showed an increase in the contact angles. This reason behind this type of behavior is unclear. The theory stated by Teklu et al. (2014), that a lowered IFT in low saline brine-crude oil systems upon dissolving CO_2 brings a reduction in the contact angles of the oil-low salinity brine-rock systems due to an increase in pH of the carbonated brines was not observed in this study. For a successful application of this

theory, one must know the quantity of CO_2 gas being dissolved in the brine during the pressurizing stage - something which we did not have a control on during this study due to experimental constraints. **Figure 10** shows the results of contact angle measurements for CO_2 pressurizing system.

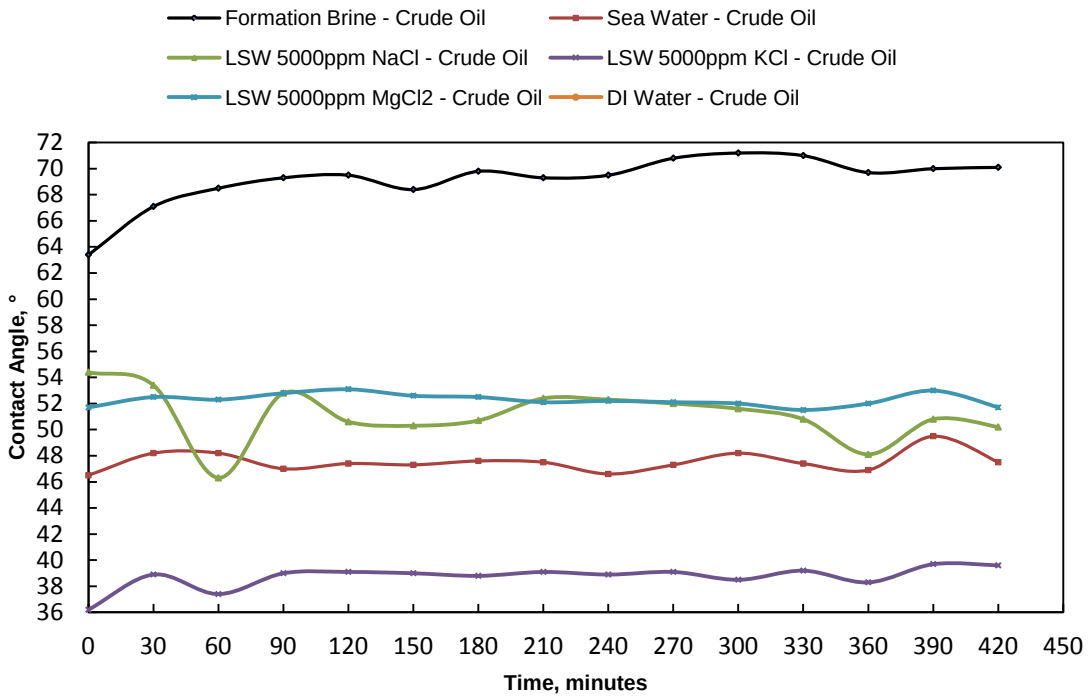

Figure 10—Contact angle measurements of fluids on Grey Bandera rock tile substrates, with CO_2 as pressurizing system T = 149°F, P = 500 psi.

5.1.3 Corefloods

Seven experiments were performed on the prepared Grey Bandera sandstone cores in the vertical orientation of the coreholder apparatus **(Table 9)**. In all the

experiments performed, early water breakthroughs were observed within injection of 1 PV, for both low salinity and high-salinity cases, due to the large viscosity differences between the injected waters and crude oil.

Experiment ID	Slug Type	Core ID	Recovery Mode	Injection Rate, cm^3/min	Slug Size, PV	Incremental Oil Recovery, %OOIP	Total Oil Recovery, %OOIP
C-1	Formation Brine (174,156 ppm)	HK-1	Secondary	0.5	5.7	18.44	18.44
				1	3	0	
C-2	Seawater (54,680 ppm)	HK-2	Secondary	0.5	5.7	21.89	21.89
				1	3	0	
C-3	KCl Solution (5,000 ppm)	HK-5	Secondary	0.5	5.7	18.57	18.57
				1	3	0	
C-4	$MgCl_2$ Solution (5,000 ppm)	HK-8	Secondary	0.5	5.7	20.87	20.87
				1	3	0	

Table 9—Summary of coreflood experiments at T = 149°F, overburden pressure = 1,600 psi and back pressure = 500 psi.

Experiment ID	Slug Type	Core ID	Recovery Mode	Injection Rate, cm^3/min	Slug Size, PV	Incremental Oil Recovery, %OOIP	Total Oil Recovery, %OOIP
C-5	NaCl Solution (5,000 ppm)	HK-6	Secondary	0.5	5.7	20.97	20.97
				1	3	0	
C-6	LSW with 5,000 ppm NaCl Solution + Immiscible CO_2 Continuous	HK-7	Secondary + Tertiary	0.5	5.7	36.32	44.02
				0.5	1.2	7.70	

Table 9 Continued

Experiment ID	Slug Type	Core ID	Recovery Mode	Injection Rate, cm^3/min	Slug Size, PV	Incremental Oil Recovery, %OOIP	Total Oil Recovery, %OOIP
C-7	LSW with 5,000 ppm NaCl Solution - Alternating - Immiscible CO_2	HK-3	Secondary 1 : 1 WAG Ratio	0.5	5.7 (Base Waterflood : 0.4 PV, 11 WAG Cycles with 0.24 PV each of CO_2 and LSW)	66.84	66.84

Table 9 Continued

The experimental conditions were similar for all experiments, maintaining an overburden pressure of 1600 psi, a back pressure at core outlet of 500 psi, and a reservoir temperature of 65°C. Fluids were injected at the bottom face and produced from the top face. The experiments were namely:

C-1: Formation waterflooding as secondary recovery mode on core HK-1, with 5.7 PV injected at 0.5 cm^3/min followed by 3 PV injected at 1 cm^3/min.

C-2: Sea waterflooding as secondary recovery mode on core HK-2, with 5.7 PV injected at 0.5 cm^3/min followed by 3 PV injected at 1 cm^3/min.

C-3: LSW of 5,000 ppm KCl solution as secondary recovery mode on core HK-5, with 5.7 PV injected at 0.5 cm^3/min followed by 3 PV injected at 1 cm^3/min.

C-4: LSW of 5,000 ppm $MgCl_2$ solution as secondary recovery mode on core HK-8, with 5.7 PV injected at 0.5 cm^3/min followed by 3 PV injected at 1 cm^3/min.

C-5: LSW of 5,000 ppm NaCl solution as secondary recovery mode on core HK-8, with 5.7 PV injected at 0.5 cm^3/min followed by 3 PV injected at 1 cm^3/min.

C-6: LSW of 5,000 ppm NaCl solution as secondary recovery on core HK-7, with 5.7 PV injected at 0.5 cm^3/min, followed by 3 PV of continuous immiscible CO_2 injection.

C-7: LSW-alternating-immiscible CO_2 flooding as secondary recovery mode with 5,000 ppm NaCl solution on core HK-3, with 5.7 PV injected at 0.5 cm^3/min.

5.1.3.1 Effect of Salinity of Injected Brine on Oil Recovery during Waterflooding

Seawater (54,680 ppm) used in experiment C-2 yielded the highest oil recovery of 21.89% OOIP among all experiments, which was an additional 3.45% over the base case of formation waterflooding (174,156 ppm) in experiment C-1 that yielded an 18.44% recovery of OOIP. Among the three low-salinity waterflooding cases performed, all three scenarios yielded a higher oil recovery than formation waterflooding. Those were namely 5,000 ppm NaCl solution in experiment C-5 yielding a total RF of 20.97 % OOIP, followed by 5,000 ppm $MgCl_2$ solution in experiment C-4 with an RF of 20.87%

OOIP, and 5,000 ppm KCl solution in experiment C-3, resulting in an RF of 18.57% OOIP. From the injection of a lower salinity water potential point of view, decreasing the salinity did increase the recovery factor for all of the cases performed on Grey Bandera Sandstones, when compared to conventional waterflooding, by an additional margin varying between 0.13% and 3.45%. In the low salinity cases, oil production was observed for a longer period of time. For example, in experiment C-5 with 5,000 ppm NaCl solution, the oil was produced until the injection of 2.4 PV, and for the Sea waterflooding case in experiment C-2, oil was produced until the injection of 1.75 PV. However, in the case of formation waterflooding as in experiment C-1, oil was produced until the injection of 1.25 PV. An inverse relation was seen in oil production period with decreasing salinity.

5.1.3.2 Effect of Fines Migration during Waterflooding

Based on the pressure drop shown in **Figures 11**, the high-salinity formation waterflooding did not create any potential fines migration during the course of the experiments. **Figure 12** shows the incremental and cumulative oil volumes for the same.

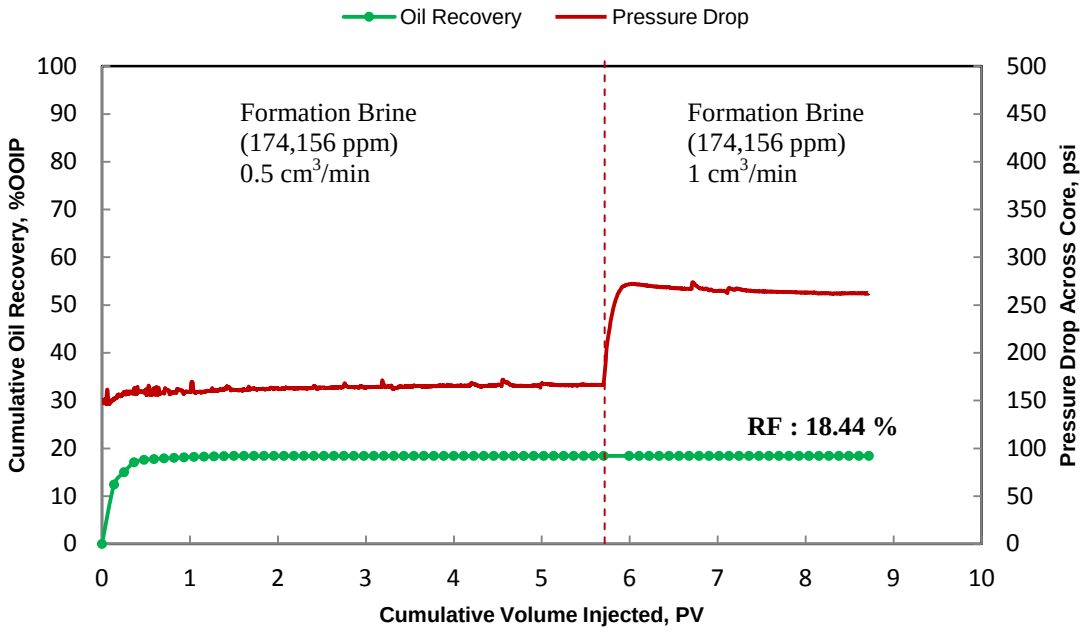

Figure 11—Oil RF and pressure drop across the core HK-1 for experiment C-1.

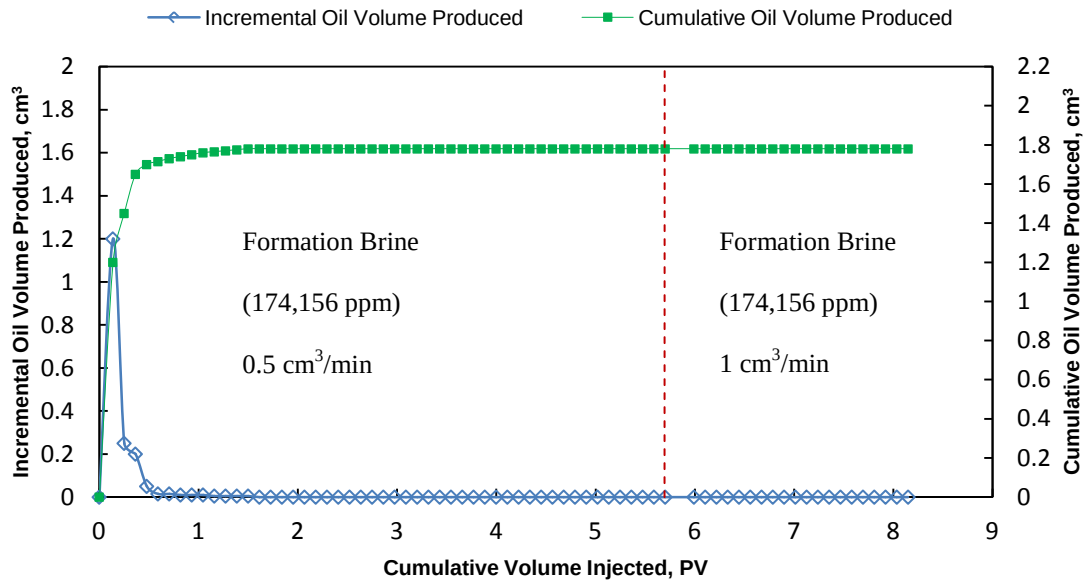

Figure 12—Incremental oil volumes and cumulative oil volumes recovered from the core HK-1 for experiment C-1.

Likewise, a similar trend in pressure drop for sea waterflooding is seen in **Figure 13**, and incremental, cumulative volumes for the same in **Figure 14**. The pressure drops were stable throughout the experiment for a given rate in both cases. When formation water was injected, the EDL is potentially compressed, thus avoiding any reason for mobilizing fines. In the case of seawater injection, fines mobilization might have been present due to a reduction in salinity, but definitely far lesser in degree than that of the 5,000 ppm low saline water cases.

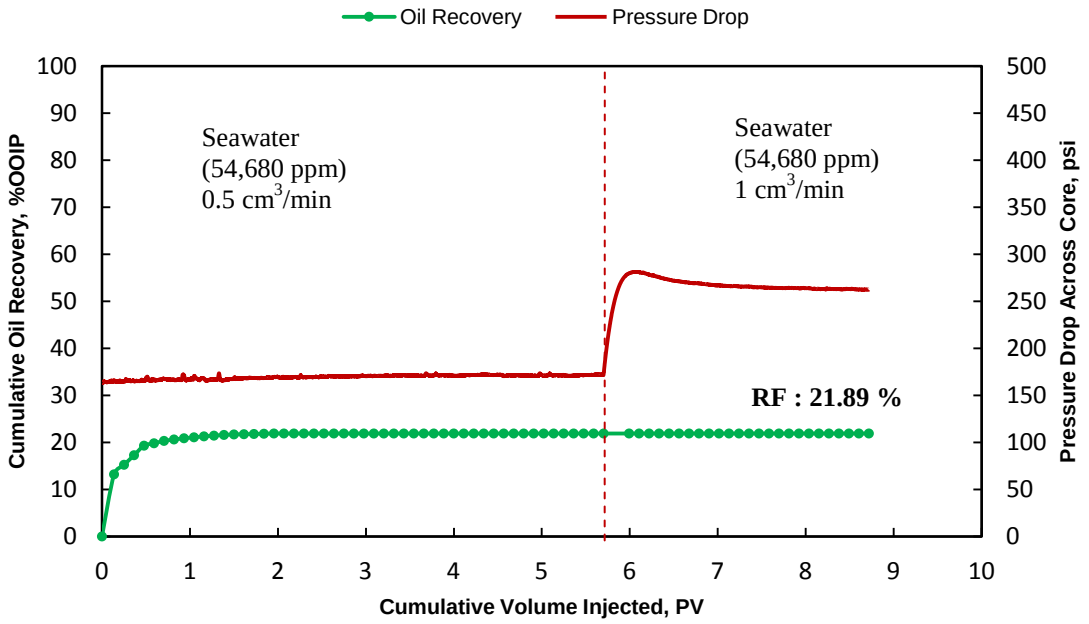

Figure 13—Oil RF and pressure drop across the core HK-2 for experiment C-2.

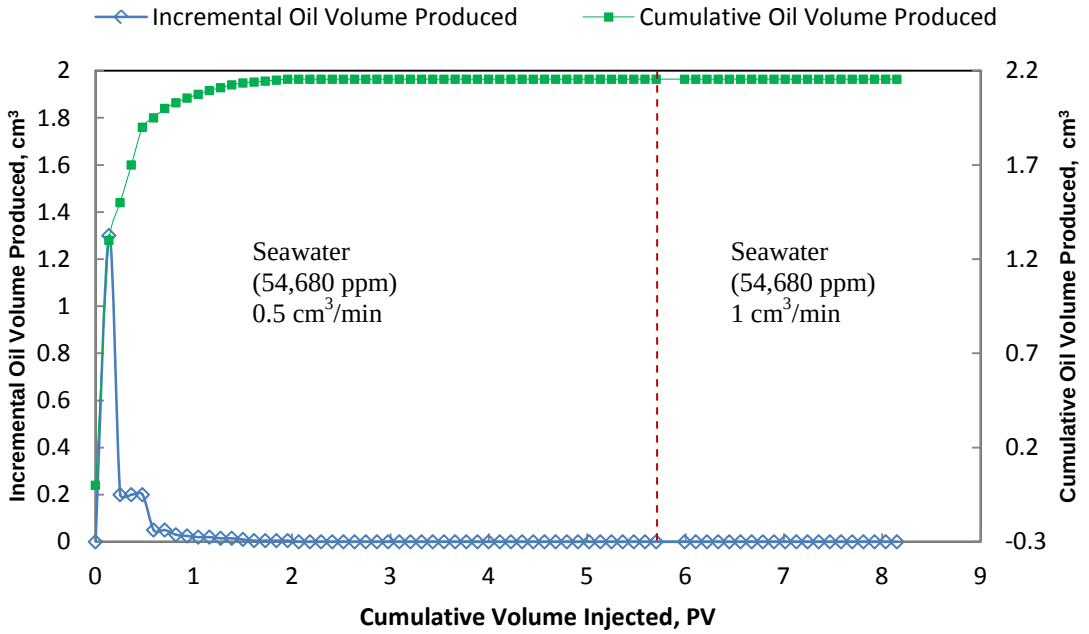

Figure 14—Incremental oil volumes and cumulative oil volumes recovered from the core HK-2 for experiment C-2.

Figures 15 and **16** show the oil RF, pressure drop, and incremental, cumulative volumes for monovalent KCl solution flooding.

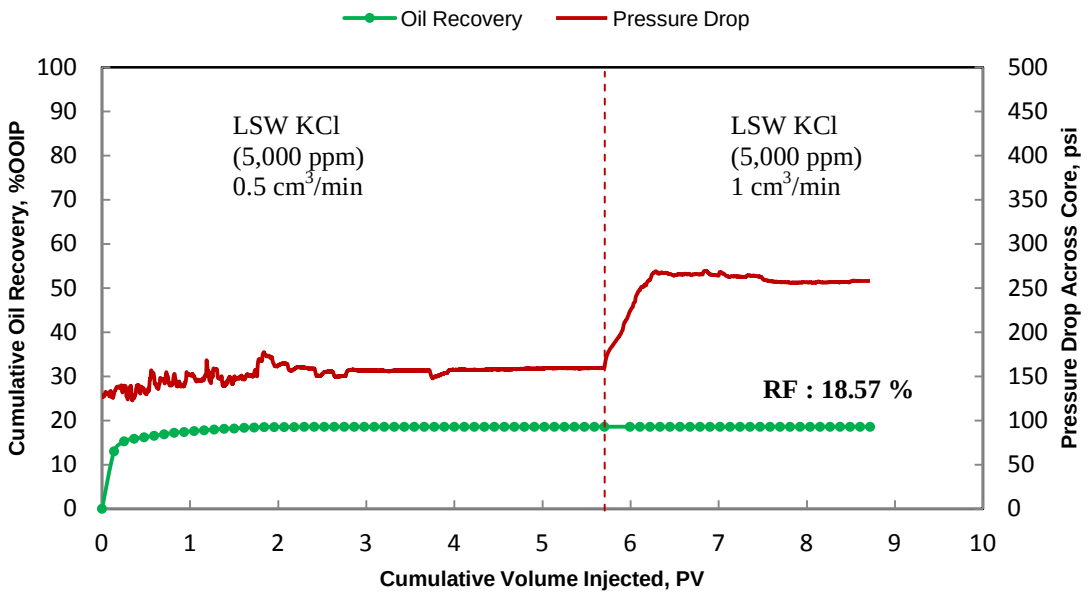

Figure 15—Oil RF and pressure drop across the core HK-5 for experiment C-3.

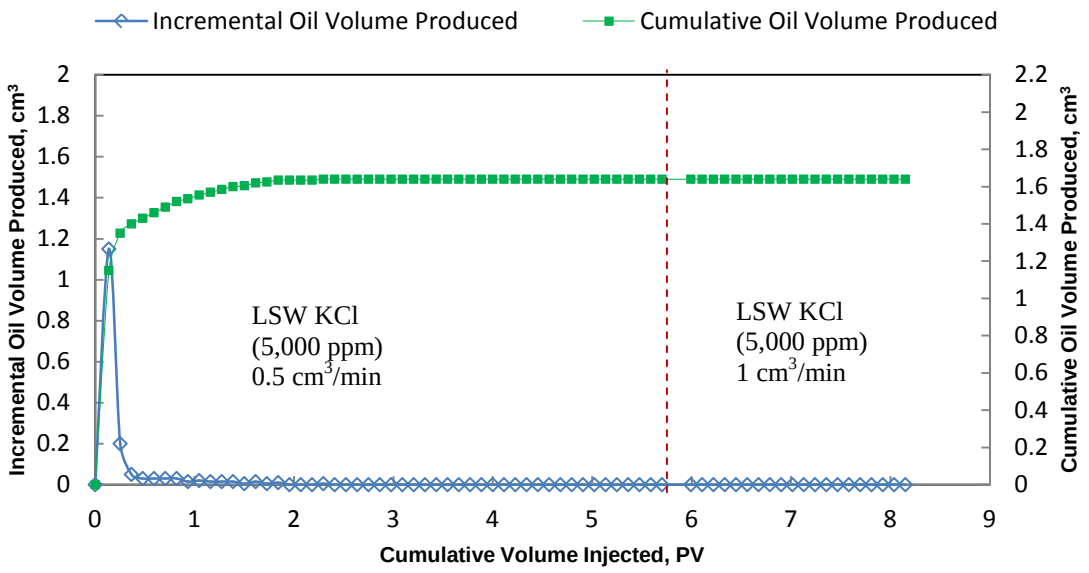

Figure 16—Incremental oil volumes and cumulative oil volumes recovered from the core HK-5 for experiment C-3.

In the cases of low-salinity brines with 5,000 ppm salt concentrations, divalent $MgCl_2$ was seen to have a lesser degree of fines migration, as observed in the pressure drop plot in **Figure 17**.

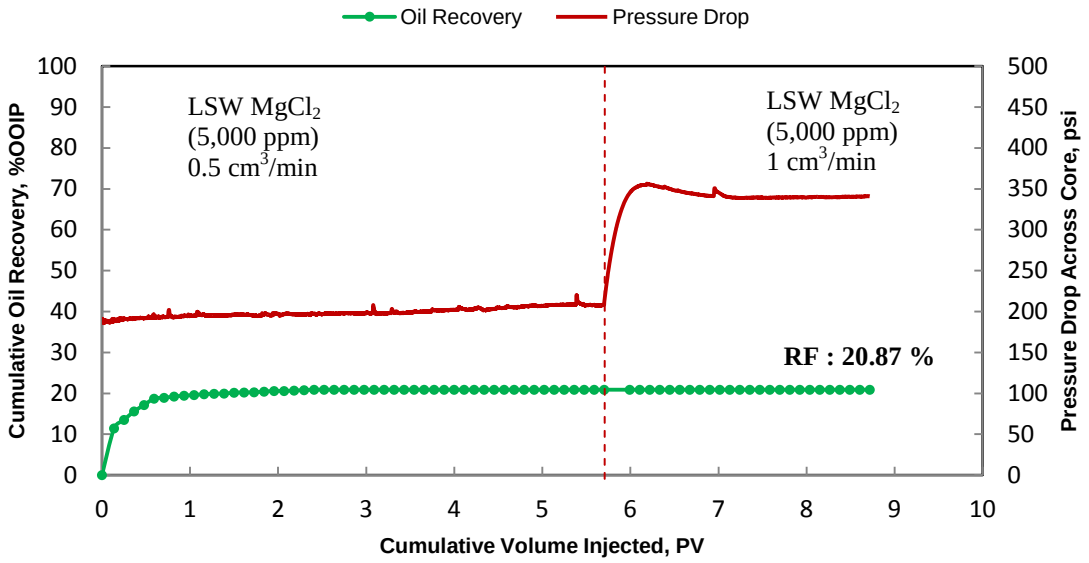

Figure 17—Oil RF and pressure drop across the core HK-8 for experiment C-4.

Monovalent KCl and NaCl solutions seemed to yield a greater degree of fines migration as the pressure drop profiles, show an overall increase through the course of water injection during the experiments. An increased fines migration scenario results in the plugging of larger pores by mobilized clays, thus directing injected waters to smaller pores and consequently increasing sweep efficiency of oil in the cores. **Figure 18** shows the incremental and cumulative volumes for $MgCl_2$ solution flooding.

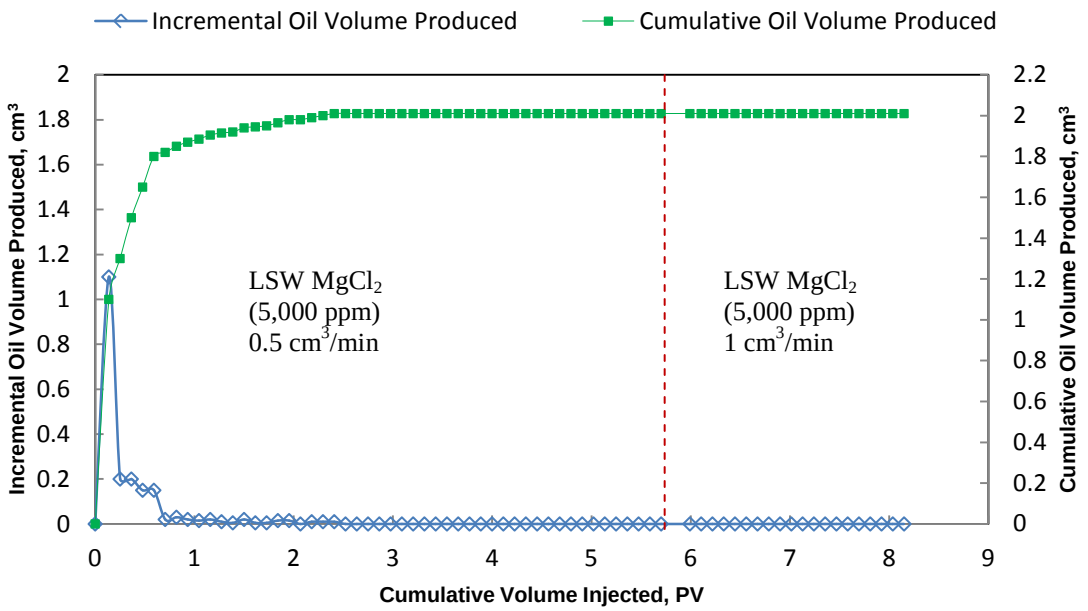

Figure 18—Incremental oil volumes and cumulative oil volumes recovered from the core HK-8 for experiment C-4.

Figures 19 and **20** show the oil RF, pressure drop, and incremental, cumulative volumes for monovalent NaCl solution flooding.

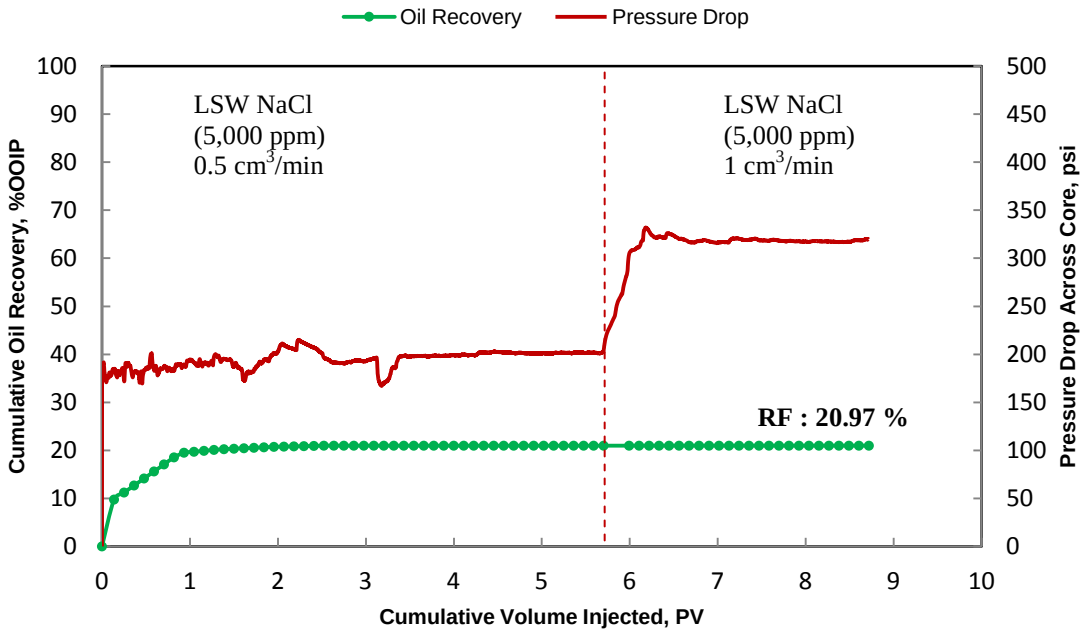

Figure 19—Oil RF and pressure drop across the core HK-6 for experiment C-5.

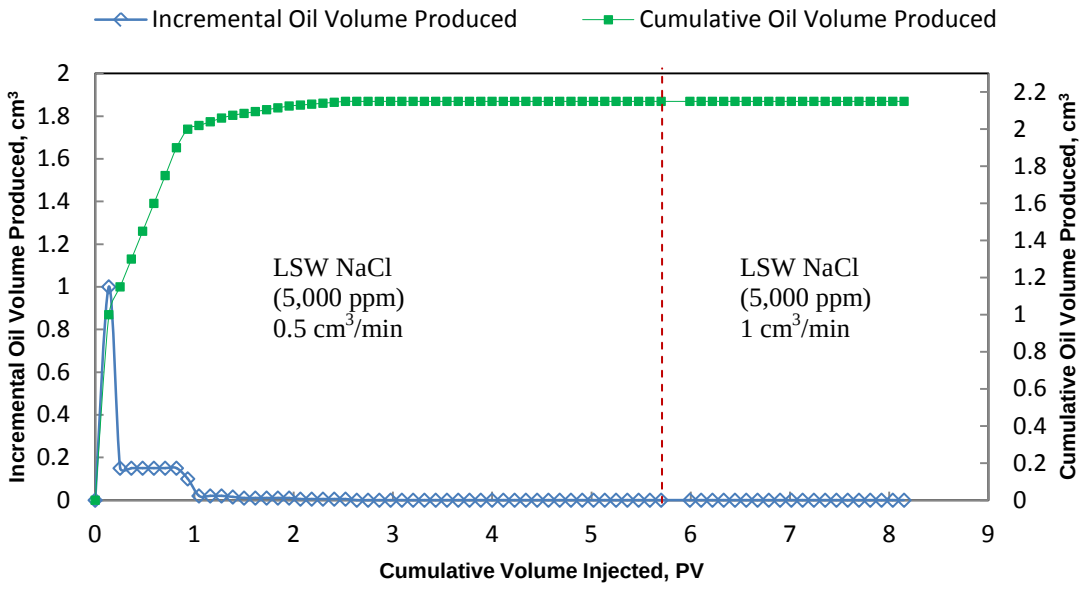

Figure 20—Incremental oil volumes and cumulative oil volumes recovered from the core HK-6 for experiment C-5.

5.1.3.3 Effect of Free Cations on Oil Recovery during Low-Salinity Waterflooding

Two monovalent cations and one divalent cation have been tested in the injected low-salinity waterflooding cases.

Monovalent NaCl solution proved to be the most effective, and this is attributed to the possible mechanism of MIE during waterflooding, with free Na^+ cations displacing and substituting for the divalent Ca^{2+} and Mg^{2+} cations attached to clays.

Monovalent KCl solution was tested to see whether K being higher than Na in the chemical reactivity series had any effect in replacement of the divalent cations during the potential MIE mechanism. However, it was only mildly more efficient than formation waterflooding, and was much lesser in oil recovery than that of the 5,000 ppm NaCl solution case. K^+ ions were absent in the initial connate water. A higher degree of fines migration occurred in this case as explained before, when compared to 5,000 ppm NaCl solution injection. Therefore, even though the EDL expansion and MIE processes may have been at work to release the clay and oil minerals, the formation clay may not have readily accepted K^+ ions as it did with Na^+. The rock surface and connate water ions develop an ionic equilibrium overtime, due to which it is ideal that the injected water comprises of familiar salt species to that of connate water. Divalent cations in $MgCl_2$ solution were as effective as the monovalent cations in NaCl solution. The EDL expansion mechanism is attributed to this process.

5.1.3.4 Effect of Rock Wettability on Oil Recovery during Waterflooding with Different Injected Brines

All waterflooding cases performed were established under the water-wet category, based on the contact angle experimental results. On a relative basis, low-salinity brines were more water-wet, and proved more efficient in recovering OOIP, as compared to the formation waterflooding case. Result revealed no exact trend between the degree of water wetness among the different low-salinity brines themselves and their corresponding RF's. Sea waterflooding oil RF was not in exact coordination with the degree of water wetness. Sea waterflooding yielded a less water-wet state than formation waterflooding, and all the low-salinity brine systems, based on contact angle experiments, and yet yielded the highest RF's in corefloods. This observation was in accordance with a study conducted by Tang et al. (1999), who summarized that in high saline bulk surroundings, an increase in cation valence tends to decrease water-wetness, but the corresponding oil recovery by waterflooding tends to increase. Seawater seemed to have a more optimum salinity concentration in comparison to lower saline cases and formation brine, as evident from the IFT studies. Low IFT values for crude oil-brine phases result in reduced capillarity during waterflooding which leads to increased oil production. A combination of effects of the low salinity waterflooding mechanisms along with reduced IFT values between oil and seawater phases could have resulted in an overall increased oil production for this case. Although wettability alteration by low salinity waterflooding to a more water wet state is said to yield the highest oil recoveries, this effect seemed to be less effective in terms of increased oil production in the

naturally water wet Grey Bandera rocks. A low but nearly optimum salinity concentration of 54,680 ppm, as in the seawater, was more ideal for waterflooding when compared to 5,000 ppm low saline waters in this study.

5.1.3.5 Effect of Salinity of Injected Brine on Relative Permeability End Points during Waterflooding

All cores initially contained connate water with high-salinity formation brine. When seawater or low-salinity brine were injected, the Krw (Relative Permeability to Water) at Sor (Residual Oil Saturation) was similar in both these cases, but there was around a 60 percent reduction in Krw at Sor due to lowering the salinities in comparison to formation brine. **Table 10** shows the experimentally measured relative permeability end points.

Experiment ID	Mechanism	Core ID	Kabs to Formation Brine	Swirr	Sor	Keo at Swirr	Kew at Sor or Keg at Slr	Kro* at Swirr with Keo at Swirr as base	Krw* at Sor with Keo at Swirr as base
C-1	Secondary Formation Brine Flooding	HK-1	6.38	0.38	0.51	2.65	0.40	1	0.151
C-2	Secondary Sea waterflooding	HK-2	6.54	0.35	0.50	4.64	0.31	1	0.066
C-3	Secondary LSF with 5,000 ppm KCl Solution	HK-5	5.91	0.41	0.48	3.47	0.27	1	0.077
C-4	Secondary LSF with 5,000 ppm $MgCl_2$ Solution	HK-8	6.13	0.39	0.48	3.12	0.21	1	0.067

Table 10—Experimentally measured oil-water relative permeability curves' end points.

Experiment ID	Mechanism	Core ID	Kabs to Formation Brine	Swirr	Sor	Keo at Swirr	Kew at Sor or Keg at Slr	Kro* at Swirr with Keo at Swirr as base	Krw* at Sor with Keo at Swirr as base
C-5	Secondary LSF with 5,000 ppm NaCl Solution	HK-6	6.17	0.32	0.53	3.26	0.22	1	0.067

Table 10 Continued

5.1.3.6 Effect of LSW-Immiscible CO_2 Hybrid Techniques on Oil Recovery

This research included two experiments with CO_2 and LSW using hybrid techniques. Experiment C-6 was performed to test the effectiveness of a tertiary flood of continuous immiscible CO_2 injection, and C-7 was performed to test the effectiveness of secondary LSW-alternating-immiscible CO_2 injection technique. In C-7, a total of 5.7 PV of fluids were injected to compare the performance with other secondary waterflooding cases at the similar rate of 0.5 cm^3/min. A total of 11 WAG (Water-Alternating-Gas) fluid cycles were injected. Initially a base low salinity waterflood of 0.4 PV was injected, followed by equal volumes of 0.24 PV each of CO_2 and LSW.

From experiment C-6, tertiary continuous CO_2 injection was effective, as it increased the oil RF by an additional 7.7% from the base secondary low-salinity waterflooding, giving an overall recovery of 44.02% OOIP. Experiment C-7 proved the LSW-alternating-immiscible CO_2 injection to be extremely effective in the low-permeability sandstones, yielding an oil recovery of 66.84% OOIP during the injection of just 5.7 PV, with more crude oil capable of being recovered upon continuing the injection. This proves that a more optimized sweep efficiency is achieved in the case of experiment C-7. In large-scale reservoirs, the volume of CO_2 injected can be minimized for obtaining increased efficiencies via WAG processes. The effective permeability to CO_2 gas at residual liquid saturation from C-6 was measured to be 0.031 md. **Figures 21** to **24** show pressure drop and oil recovery profiles for experiments C-6 and C-7, respectively.

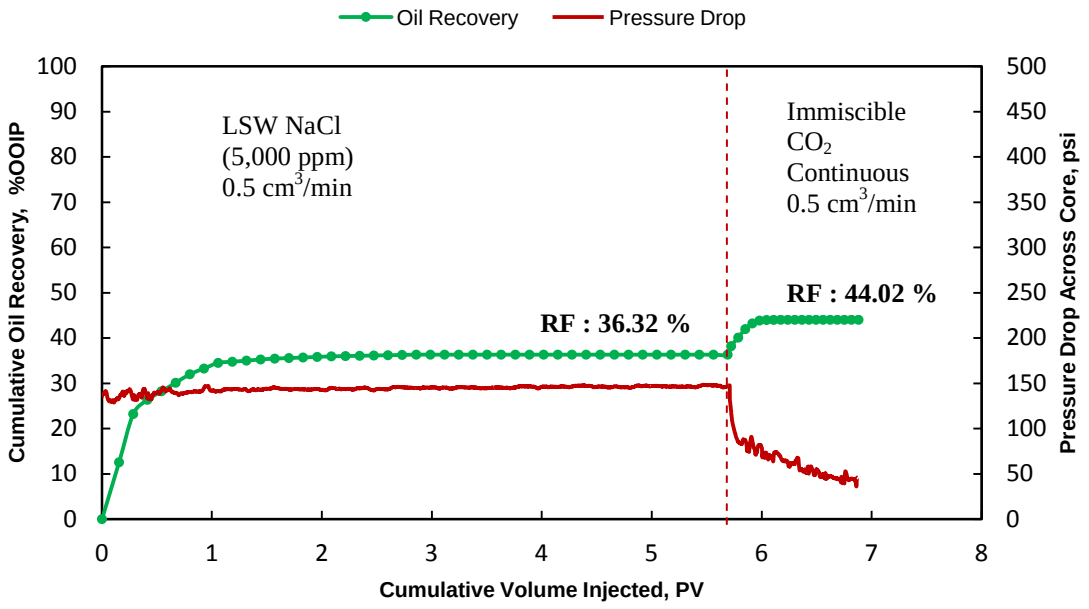

Figure 21—Oil RF and pressure drop across the core HK-7 for experiment C-6.

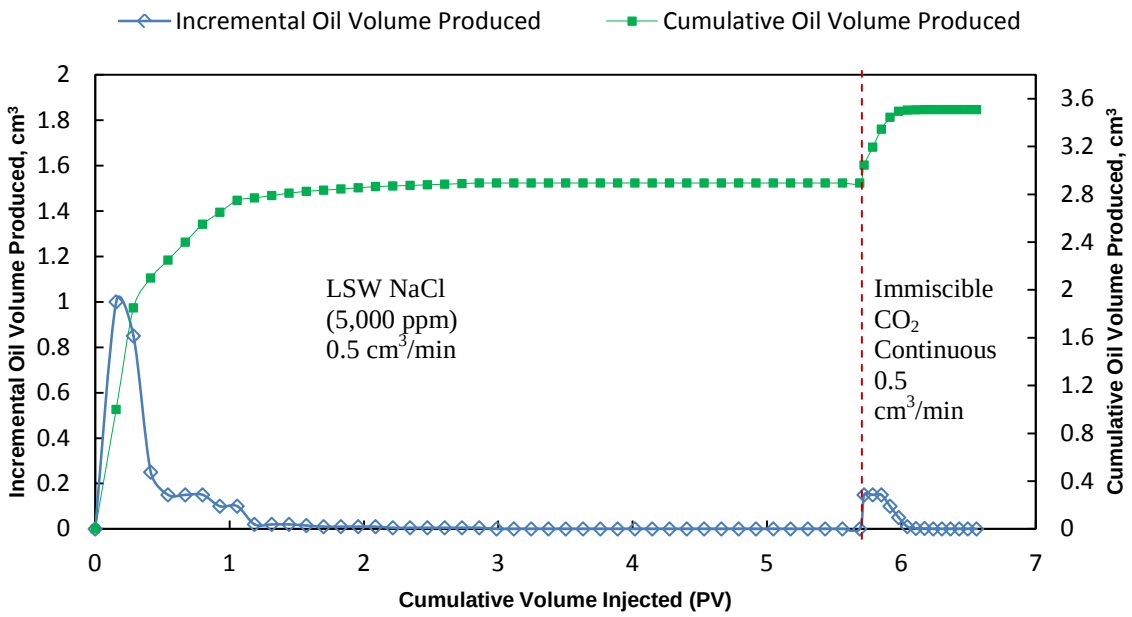

Figure 22—Incremental oil volumes and cumulative oil volumes recovered from the core HK-7 for experiment C-6.

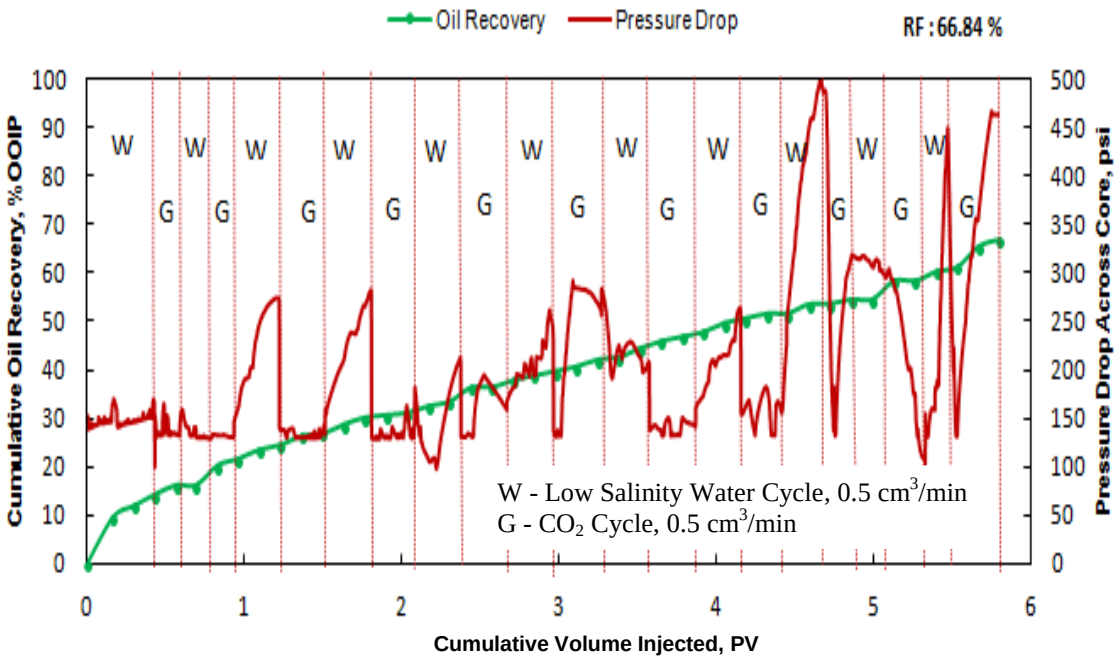

Figure 23—Oil RF and pressure drop across the core HK-3 for experiment C-7.

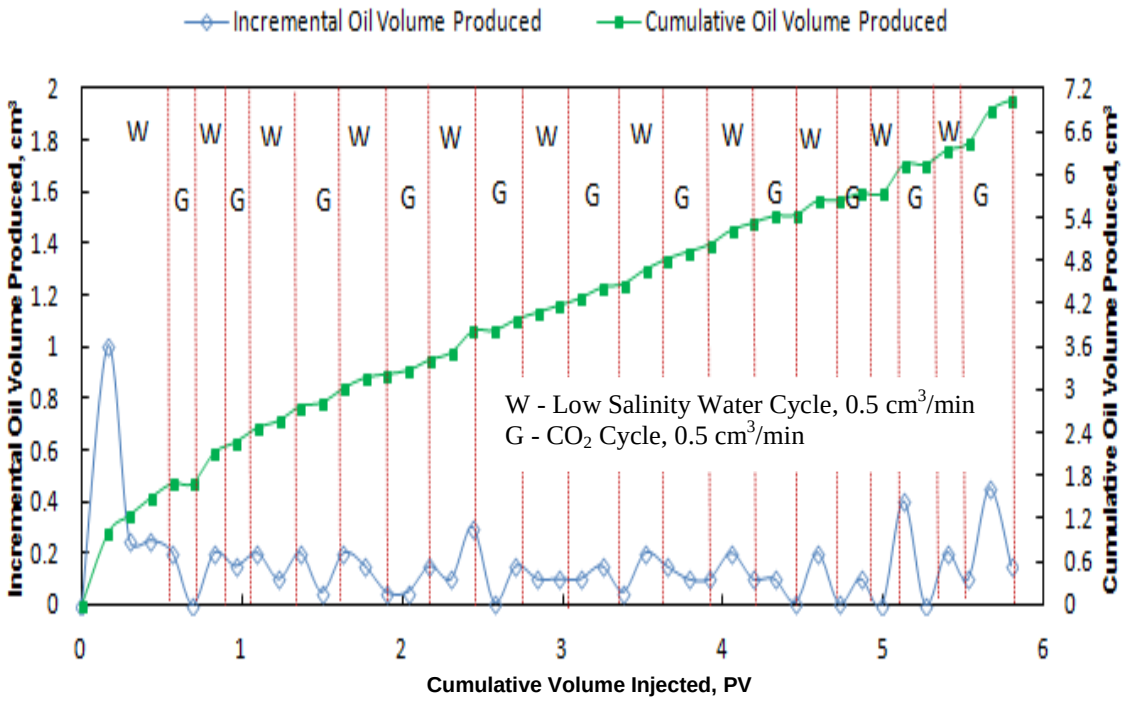

Figure 24—Incremental oil volumes and cumulative oil volumes recovered from the core HK-3 for experiment C-7.

5.1.3.7 Effect of Initial Connate Water Saturation on Oil Recovery during Secondary Low-Salinity Waterflooding

In experiment C-6, the secondary low-salinity 5,000 ppm NaCl waterflooding sequence was performed on a core with Swirr (Irreducible Water Saturation) = 0.49, and the same LSW was injected in C-5 for a core with Swirr = 0.32. For an injection of 5.7 PV of LSW at 0.5 cm^3/min, C-6 yielded 36.32% of OOIP, while 20.97% OOIP was recovered in C-5. Thus, the core with a higher connate water saturation proved a much better source for oil recovery during LSW injection. This could be due to a more water-wet nature of the core in C-6 due to a higher water retention capability during the

drainage process. As a result of this, lesser volumes of crude oil are adhered to the surface of the rocks, thus available for being swept during waterflooding. This sweep efficiency combined with low salinity water potentials increase the total oil recovery factor. As evident from the pressure drop curve in **Figure 21**, it shows a limited fines migration scenario in experiment C-6. Thus a more water-wet core is less susceptible to fines migration during low salinity waterflooding.

5.2 Simulation Studies

5.2.1 History-matching

Three coreflood experiments, C-1, C-2 and C-5, were simulated and history matched **(Figures 25** to **27)**.

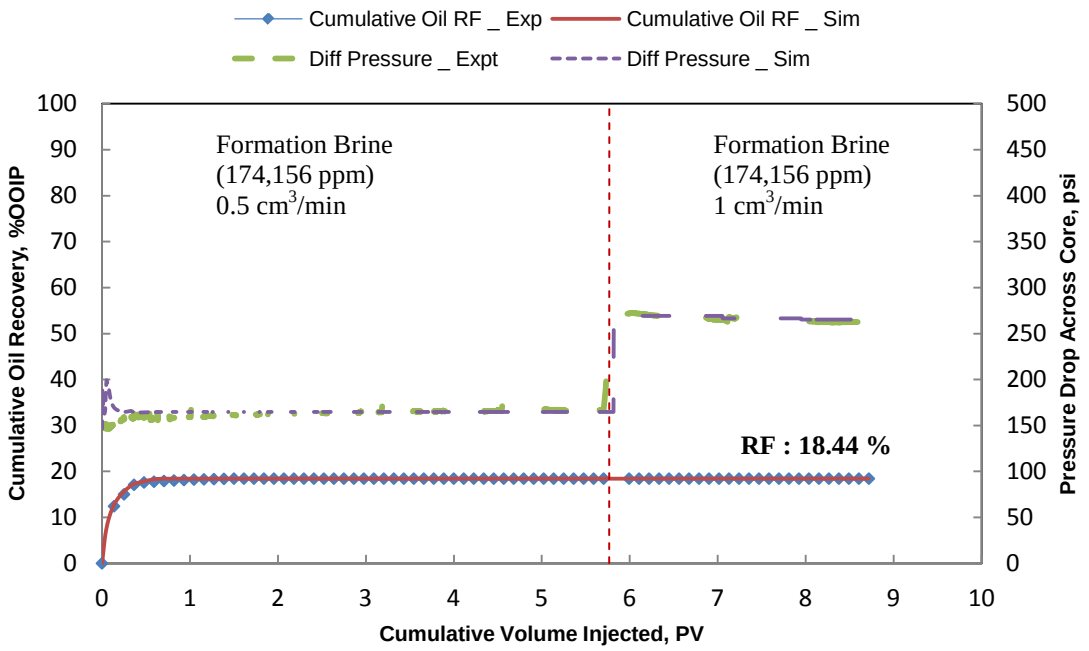

Figure 25—Experiment and simulation history match of C-1: pressure drop and oil RF% vs. PV injected.

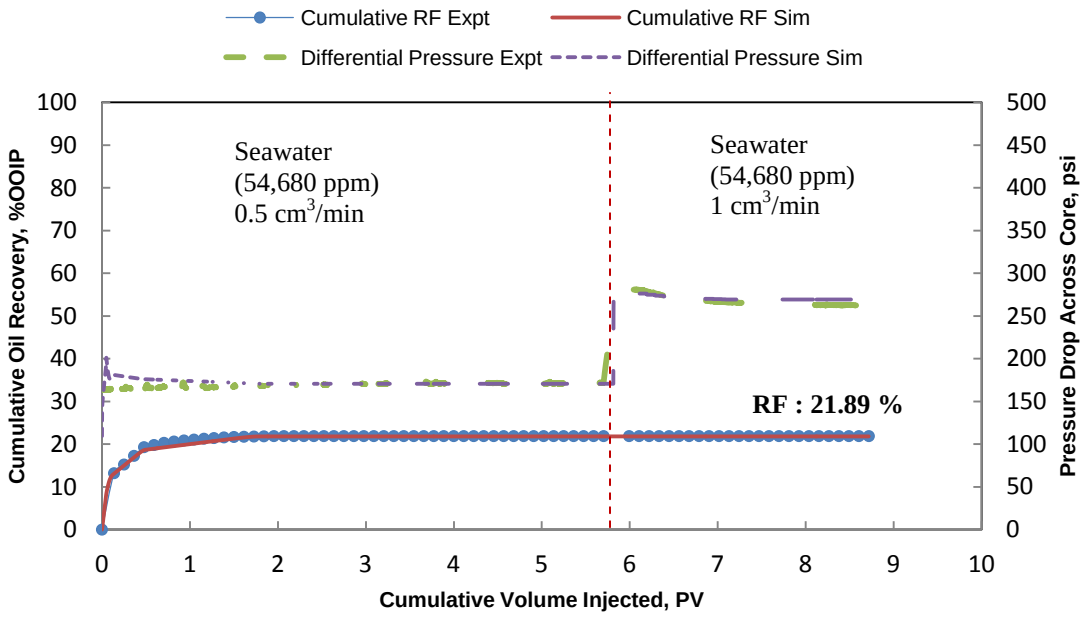

Figure 26—Experiment and simulation history match of C-2: pressure drop and oil RF% vs. PV injected.

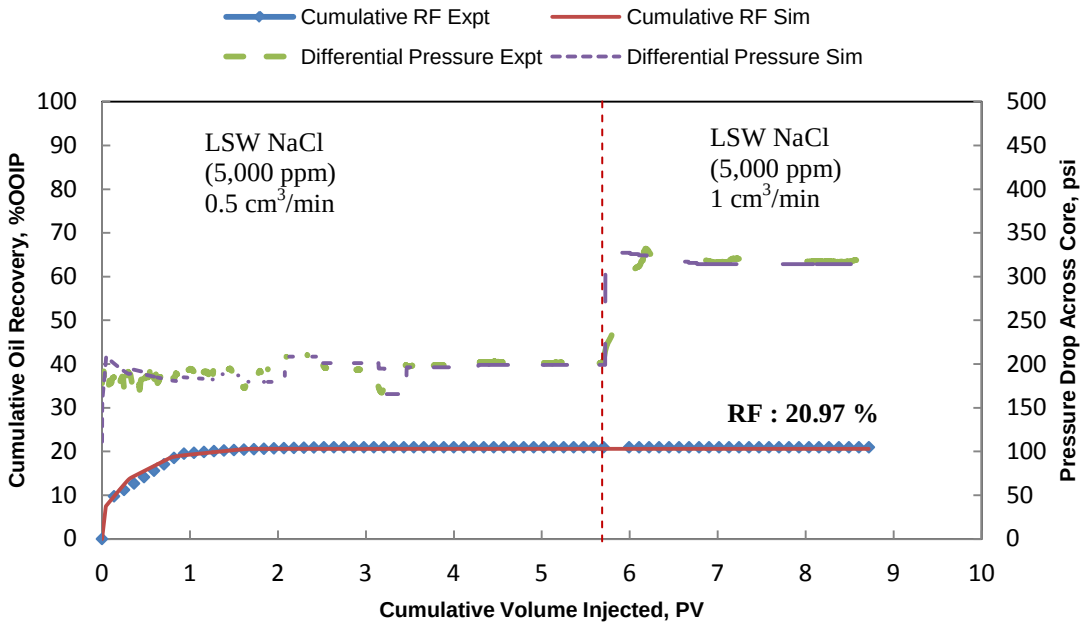

Figure 27—Experiment and simulation history match of C-5: pressure drop and oil RF% vs. PV injected.

This covered all three levels of injected water salinity used in this study. The parameters used for history-matching the results were the relative permeability curve points generated by correlations, with the oil curve end points and Swirr being treated as constants. The Krw curve points were changed to range between 0 and Kew value at Sor, as measured from the experiment. The relative permeability curves had a huge influence on the oil recovery profile. **Figures 28** to **30** show degrees of sensitivity changes made in the correlation based curves to obtain good history matches.

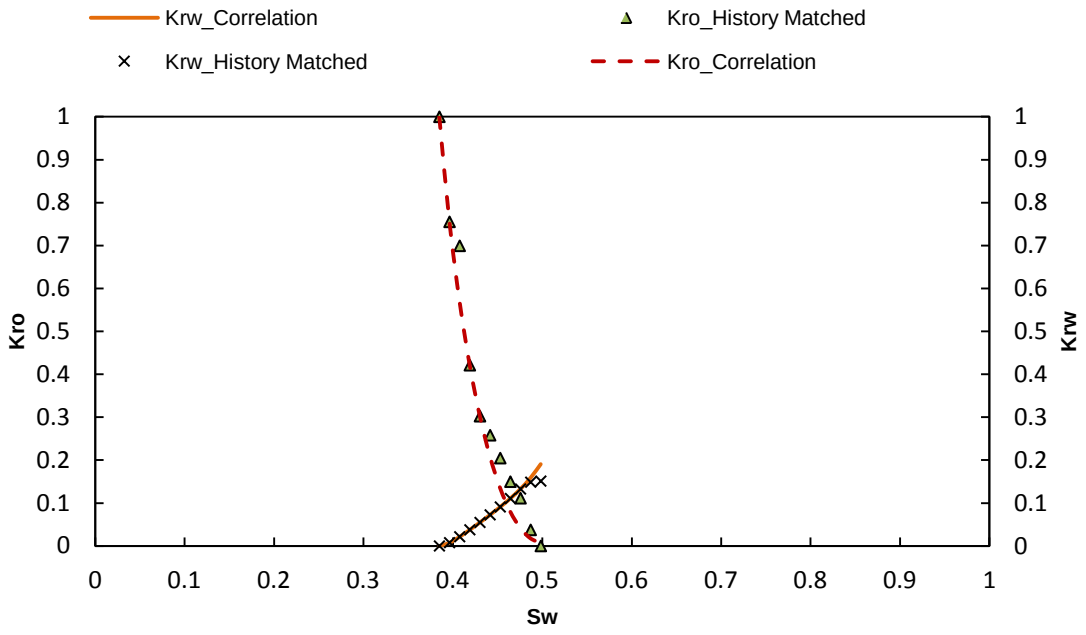

Figure 28—Correlation based relative permeability curves and history-matched relative permeability curves for experiment C-1, formation waterflooding.

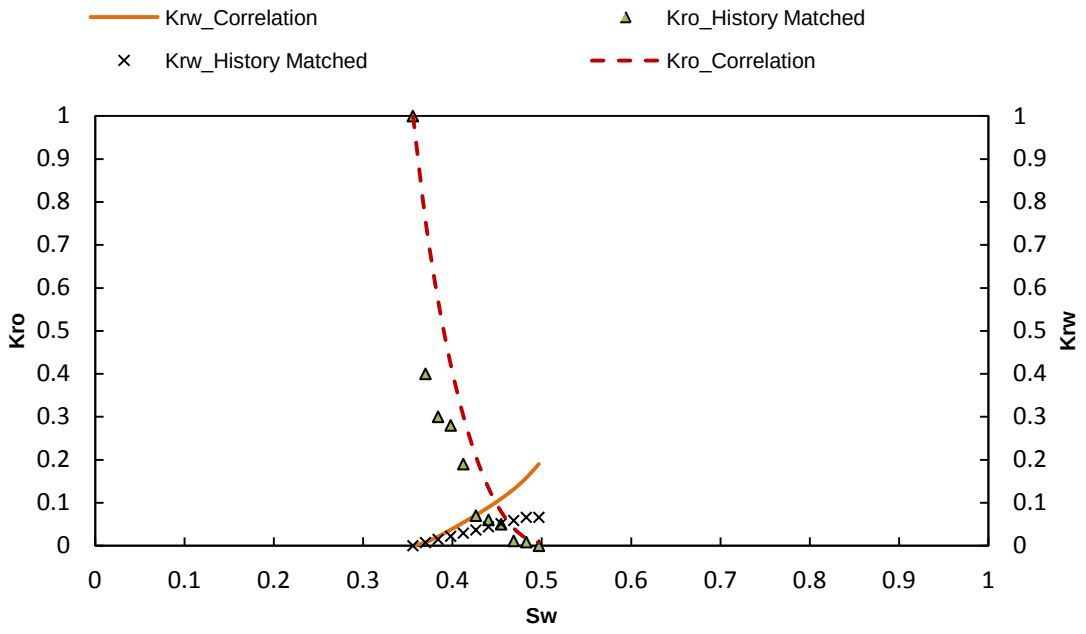

Figure 29—Correlation based relative permeability curves and history matched relative permeability curves for experiment C-2, sea waterflooding.

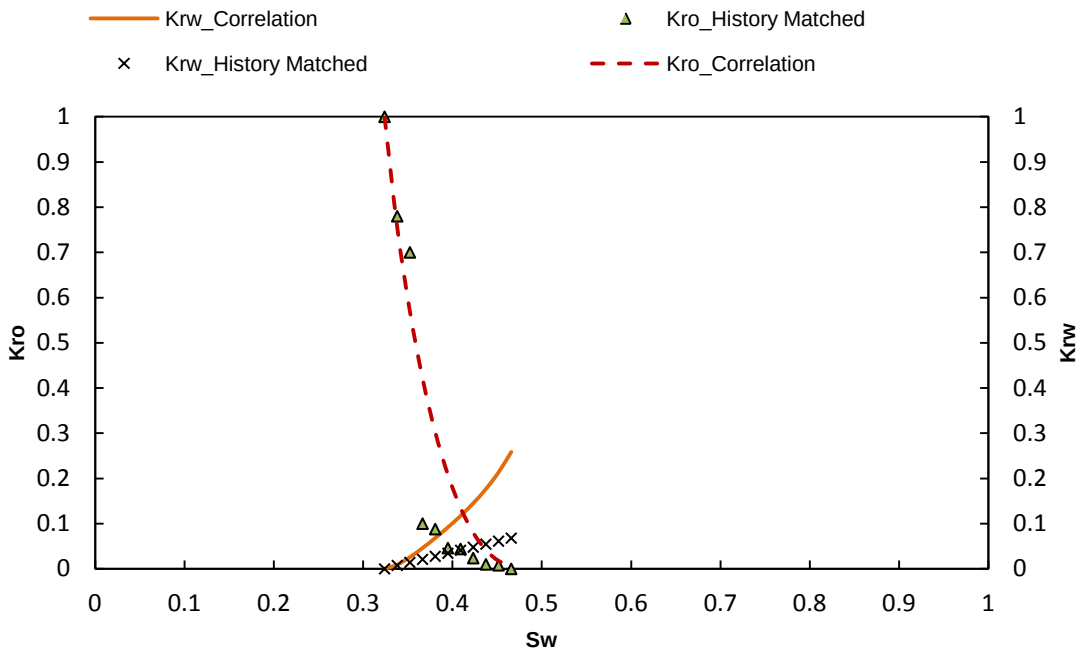

Figure 30—Correlation based relative permeability curves & history matched relative permeability curves for experiment C-5, low-salinity waterflooding.

Large transmissibility multipliers were used across the top layer cross section and the bottom layer cross section to ease entry and exit of fluids into and out of the model via the injector and the producer. This helped avoid any boundary errors and high entry pressures involved due to small cell sizes near the well connections. Transmissibility multipliers were used across the bulk of the core model to simulate permeability reduction caused due to potential fines migration within the core.

Experiment C-1 was history-matched with minor changes to the relative permeability curve points generated from the correlations. This proved the correlations to be very effective and reliable for conventional waterflooding, similar to those created by Mohamad et al. (2000) from a library of relative permeability imbibition experiments. Thus not much change in the nature of correlation-generated curves was observed in the

case of C-1. Transmissibility multipliers for the bulk of the core model were not necessary in this case, as the pressure drop profiles were stable for the entire experiment. This proved that fines migration was absent in the high-salinity waterflooding case.

Experiment C-2 and C-5 were history-matched with greater changes made to the relative permeability curve data points generated from correlations, corresponding to the reduced salinity content of the injected waters. The nature of the oil and water relative permeability curves for the low-salinity cases of C-2 and C-5 shows reduced relative permeability to oil with increasing water saturation in the cores. This is in conjunction with the nature of the oil recovery factor profile, as the slope of the oil recovery during early water injection stages is greater for a high-salinity case compared to a low-salinity case.

Contact-angle experiments clearly demonstrate that the wettability of the rock is altered to a lower water-wet state for seawater-crude oil systems, and to a more water-wet state in low salinity 5,000 ppm solution-crude oil systems on a relative comparison basis to that of formation water-crude oil systems. The Corey's relative permeability curves were used to match the history matched relative permeability curve points, to obtain the appropriate Corey's exponents. Corey's correlations are given by Equations 4 and 5.

Corey's Oil - Water Relative Permeability Correlations, by Corey (1954):

Equation 4:

$$Krw^* = Krw[Swc]\, Sw^{*Nw}$$

Equation 5:

$$Kro^{*} = \quad Kro[Swc]\,(1 - Sw^{*})^{No}$$

where, Krw = normalized relative permeability to water*

Kro = normalized relative permeability to oil*

Swc = connate water saturation

Sw = water saturation

Krw = relative permeability to water

Kro = relative permeability to oil

Sw = normalized water saturation*

Nw = Corey's water exponent

No = Corey's oil exponent

The Corey's exponents appear in **Table 11**, and **Figures 31** to **33** give the oil-water relative permeability matches between the history-matched curves and Corey's relative permeability curves, using respective Corey exponents for the three simulated cases.

Experiment ID	Mechanism	Core ID	Swirr	Sor	Kro* at Swirr	Krw* at Sor	No	Nw	$\frac{\mu_o}{\mu_w}$
C-1	Formation Brine Flooding	HK-1	0.38	0.51	1	0.151	2	1	8.3
C-2	Sea waterflooding	HK-2	0.35	0.50	1	0.066	3.5	1	9.4
C-5	LSW with 5,000 ppm NaCl Solution	HK-6	0.32	0.53	1	0.067	4.5	1	11.9

Table 11—Corey's exponents and fluid viscosity ratios.

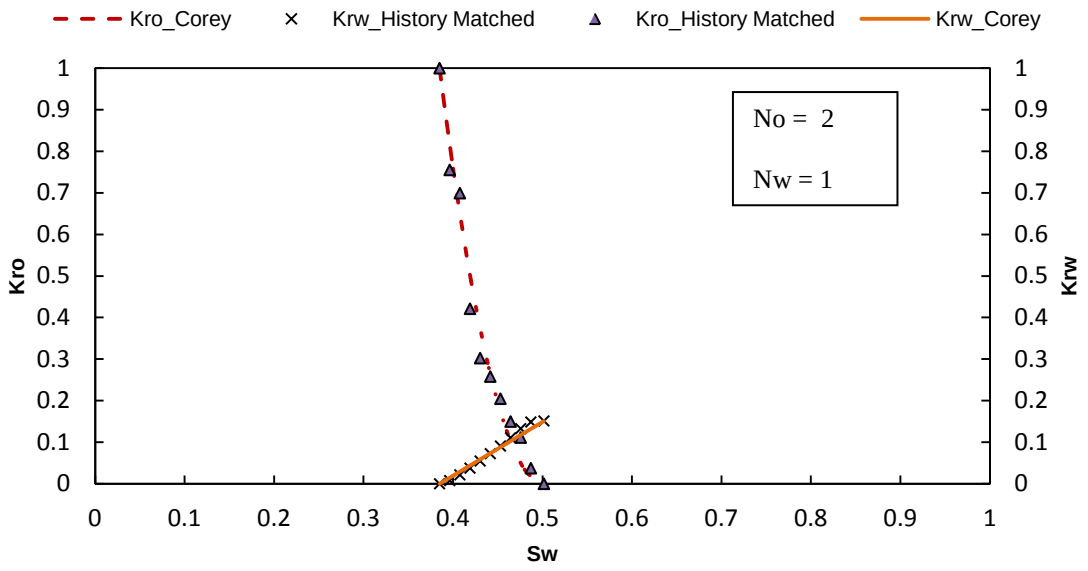

Figure 31—Corey's relative permeability curves and history matched relative permeability curves match for experiment C-1, formation waterflooding.

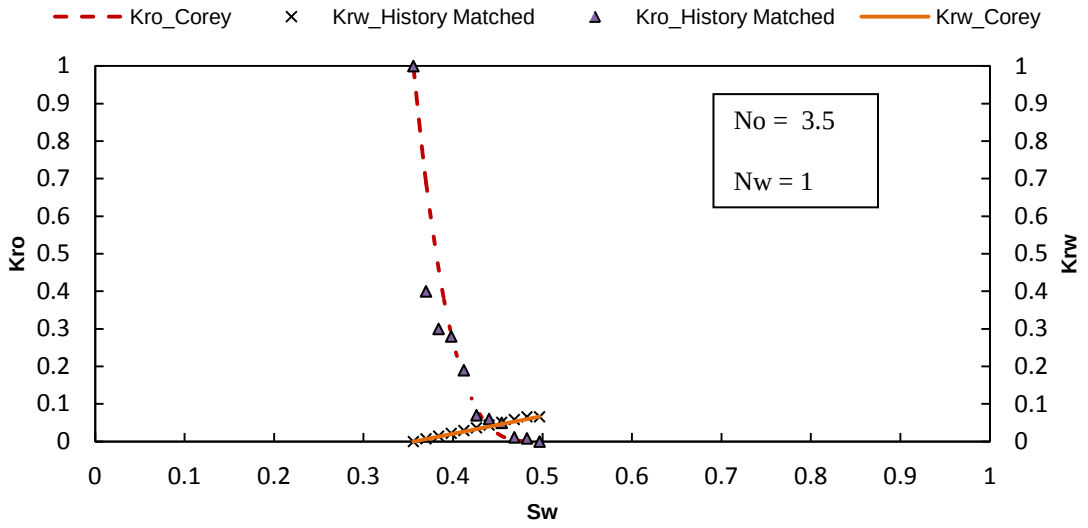

Figure 32—Corey's relative permeability curves and history matched relative permeability curves for experiment C-2, sea waterflooding.

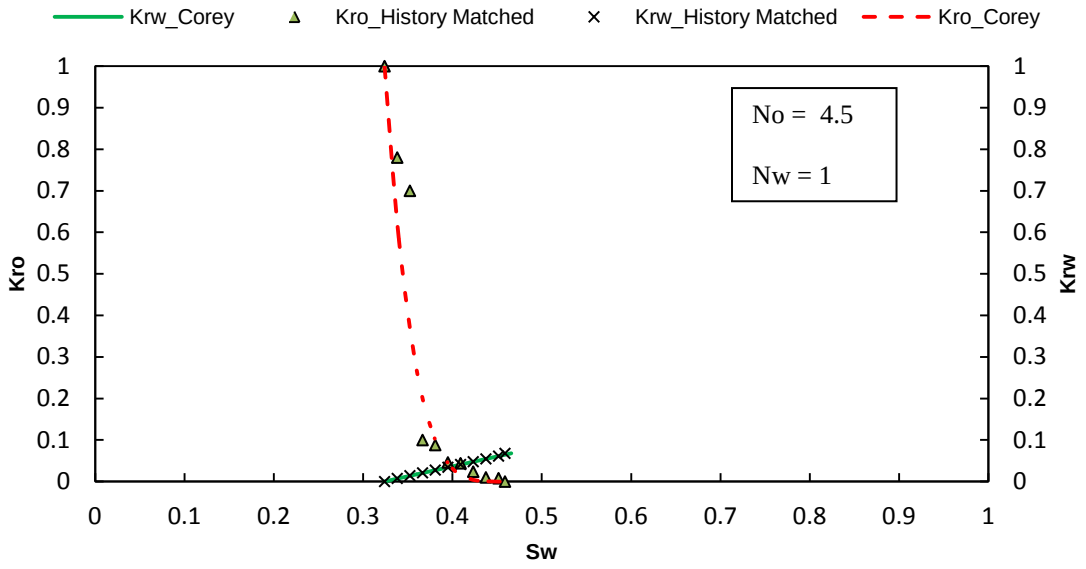

Figure 33—Corey's relative permeability curves and history matched relative permeability curves for experiment C-5, low-salinity 5,000 ppm NaCl waterflooding.

They indicate a shift in the wettability toward a less water-wet scenario being directly proportional to the reduction in injection water salinity. The nature of change in the oil relative permeability curves, as characterized by Corey's exponents, is clearly not dominated by wettability alteration between the three cases, based on wettability characterization from the experiments. They are more influenced by the injected water to crude oil viscosity ratios and the influence of fines migration which leads to further reduced relative permeabilities to the wetting and non-wetting phases, particularly in small pore sized environments such as Grey Bandera. Kevin et al. (1995) observed drastic reduced permeabilities to the oil and water phases with increasing fluid viscosity ratios to be more prominent in low-permeability reservoirs. This phenomenon was clearly observed in this study. A possible interpretation of the history-matched curves'

natures is that higher viscosity ratios shows a larger degree of variation between data points in the early water saturation periods, thus leading to a steeper fall in slope of the non wetting oil phase relative permeability curves, in comparison to the lower viscosity ratio as portrayed by a higher-salinity water-crude oil system **(Figure 34)**. This interpretation was similar to the earlier stated observation by Odeh (1959).

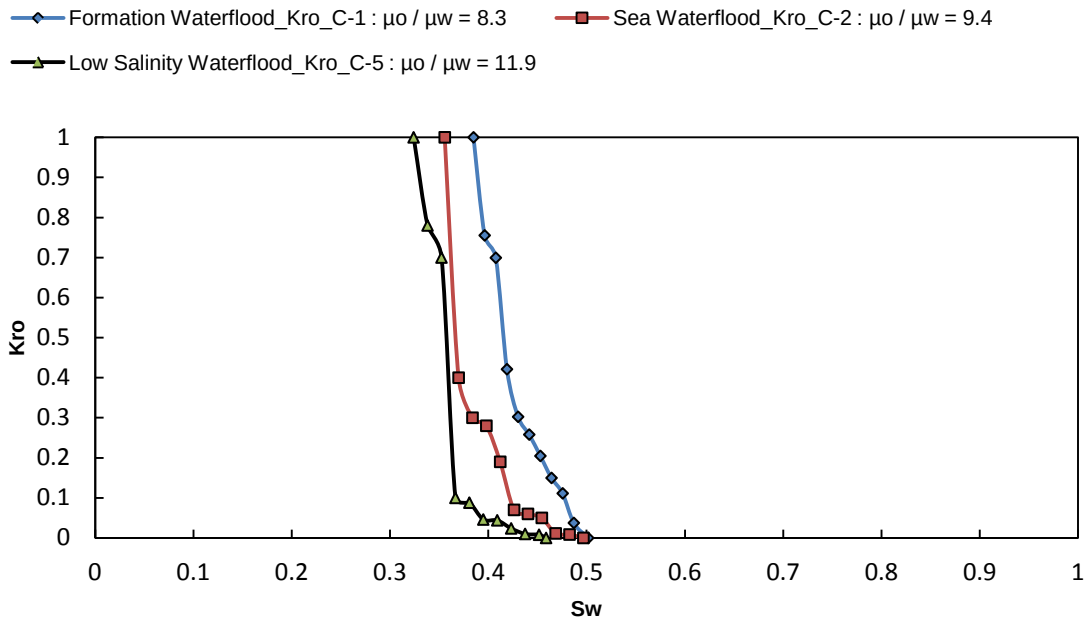

Figure 34—History matched Kro curves for experiments C-1, C-2 and C-5.

This happens due to the bypassing of the injected low-salinity brine of lower viscosity over the medium crude oil, leading to a relatively early breakthrough of water when compared to higher-salinity injected brines, as observed from the experiments. Thus, the Corey's exponents do not truly represent the wettability of the systems in this study.

Experiment C-2 did not require transmissibility multipliers in the bulk of the core model for matching the experimental pressure drop, thus proving no potential fines migration. However, in the low salinity waterflooding experiment C-5, transmissibility multipliers were used in the bulk of the core model to match pressure drop changes during the experiment. The transmissibility values were changed by a maximum extent of ±3 percent in the bulk of the model for C-5.

All three experiments proved to be of water-wet nature. **Figure 35** describes the Corey's-based curves and the changing trends in midpoint intersections with different salinity injected brines, on a normalized water saturation scale, Sw*, as previously given by Eq. (3).

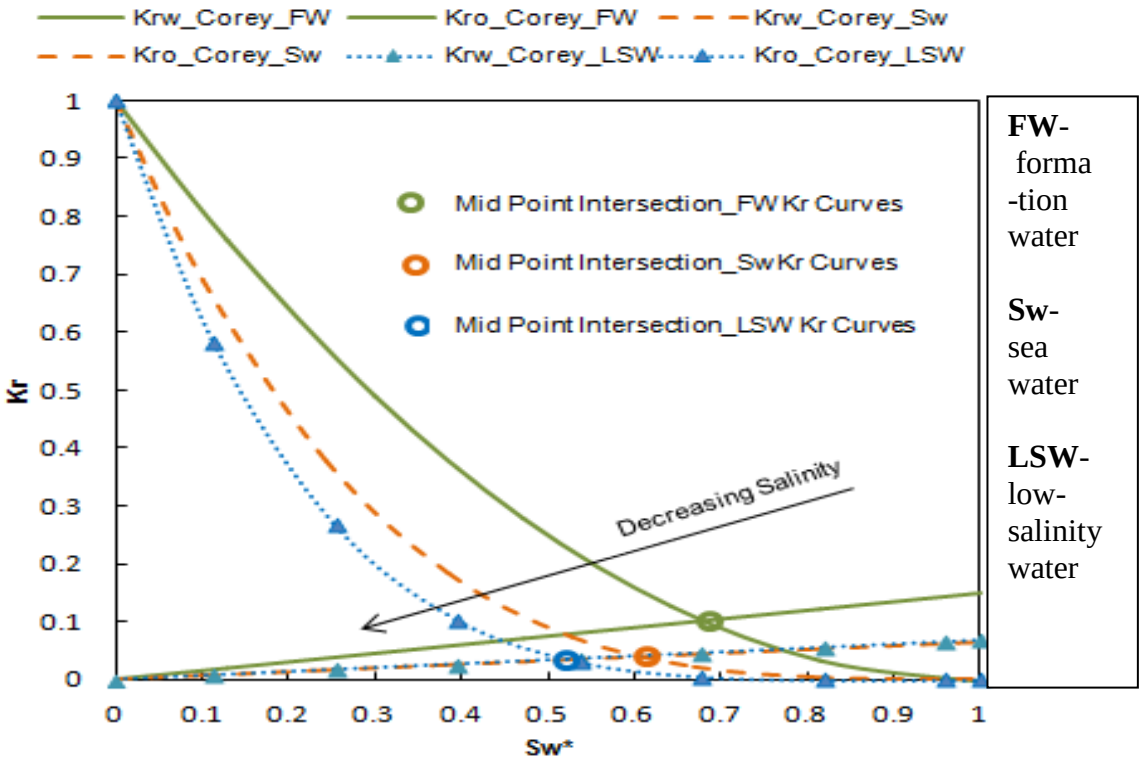

Figure 35—Trend of midpoint intersection in Corey's relative permeability curves for experiments C-1, C-2 and C-5.

Although the overall shift in the trends are toward a less water-wet scenario with decrease in salinity, the vertical shift in midpoint intersections between the non-wetting and wetting phase curves show that of a more water-wet scenario with decreasing salinity.

5.2.2 Sensitivity Study

5.2.2.1 Viscosity of Crude Oil

To verify the effect of injection water override due to high differences in fluid viscosities between the brines and crude oil, a simulation sensitivity case was performed to replicate experiment C-5, with a lighter crude oil of viscosity 1.25 cp present in the core model. As evident from **Figure 36**, decreasing the viscosity of crude oil with all other parameters remaining the same showed a quicker recovery rate of oil, with a greater oil RF slope at early injected PV. This proves the decrease in the level of bypassing of injected brines over lighter crude oils, thus leading to a more piston-like displacement.

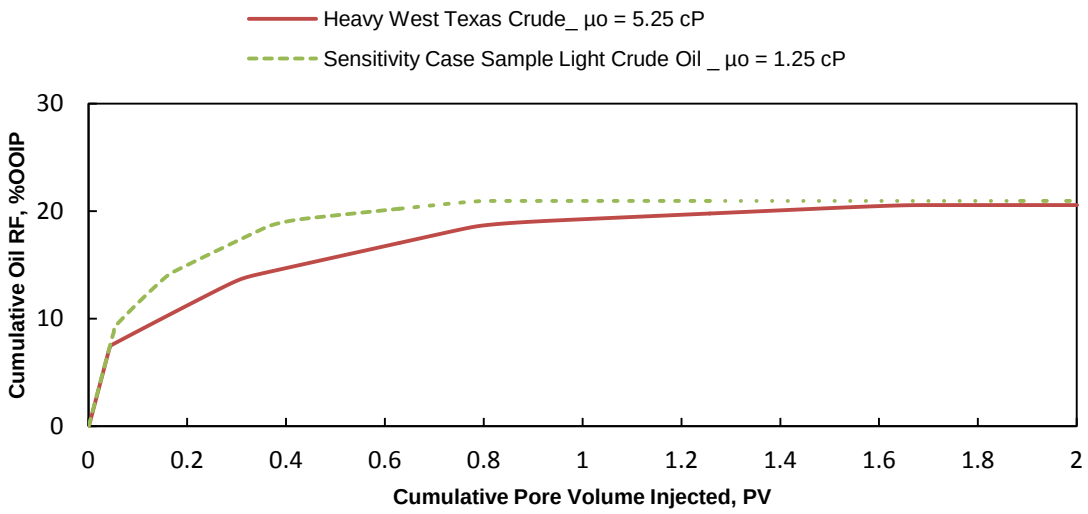

Figure 36—Simulated oil RF: C-5 low-Salinity 5,000 ppm NaCl waterflooding case for medium west Texas crude oil and sensitized light crude oil to show effect of viscosity override.

6. CONCLUSIONS

A detailed study of low-salinity waterflooding with different brines, and that of potentially incorporating CO_2 with them, has been carried out in low-permeability sandstones. Interpretation of SCAL properties using reservoir simulation as a tool to match the experimental results was conducted.

Following are the conclusions of this study:

1. Low-salinity waterflooding was marginally effective in increasing oil recovery in low-permeability, medium-oil sandstone reservoirs.
2. Seawater with 54,680 ppm proved to be the close to the optimum salinity concentration, ideal for waterflooding in this study.
3. In a large-scale field application with reservoir characteristics of this study, conventional waterflooding may be more economical in terms of secondary recovery, due to the possibility of quicker oil production in comparison to low salinity waterflooding, which may take nearly twice the time to produce as much oil as the former, owing to relative early breakthroughs.
4. Fines migration was evident during low-salinity waterflooding.
5. SCAL relative permeability curve's nature to oil was dominated by high fluid viscosity ratios and pore structures, rather than wettability alteration. Thus, Corey's exponents used for establishing oil-water relative permeability curves from simulation may not be entirely reliable in determining rock wettability during low-salinity waterflooding, due to the dominating influence of other side factors such as viscosity override and fines migration in low-permeability rocks.

6. Sandstone cores with higher initial connate water saturations were proved capable of producing more oil during low-salinity waterflooding.
7. Hybrid techniques involving immiscible CO_2 injection are an effective processes for low-permeability sandstone reservoirs, with LSW-alternating-immiscible CO_2 injection proving to be an excellent EOR technique due to high sweep efficiencies and a more controlled CO_2 mobility in the low-permeability scenarios.

7. FUTURE WORK AND RECOMMENDATIONS

As shown in the current work, low-salinity waterflooding is a complex EOR process, demanding more research studies to understand the science in complete. The existing commercial reservoir simulators are not completely capable of modeling low-salinity waterflooding to its exact mechanism. However, certain characteristics of a low-salinity waterflood are possible to be modeled, particularly the levels of mixing between injection and connate waters, and the degree of fines migration caused, using special modules in commercial reservoir simulation packages and combining these technologies. This would improve the capability to model low-salinity waterflooding in existing commercial reservoir simulators, rather than blindly depending on the input SCAL properties and transmissibility factors.

The relative permeability curves generated in this study for the various cases represent the final set of curves for a two-phase system, ignoring the difference between connate water and the injected low-salinity waters. To model the degrees of mixing of waters and fines migration, an additional set of relative permeability curves are required, by maintaining a single salt concentration in both connate and injected waters during a coreflood, and repeating the same for different levels of salinities. Thus, two or more sets of relative permeability curves are to be input into the simulator for different salinity levels, and the resultant interpolated curves would be that generated in this study, by treating several sensitivity parameters to model the physical significance taking place in real. In addition, the ion- tracking option can be used in commercial reservoir simulators to further history-match the experiments by testing the effluent fluids.

REFERENCES

Alvarado, V. and Manrique, E. 2010. Enhanced Oil Recovery: An Update Review. *Energies* **3** (9): 1529-1575.

Al-Mutairi, S. M., Abu-Khamsin, S. A., Okasha, T. M. et al. 2014. An Experimental Investigation of Wettability Alteration during CO_2 Immiscible Flooding. *Journal of Petroleum Science and Engineering* **120**: 73-77.

Austad, T., RezaeiDoust, A., and Puntervold, T. 2010. Chemical Mechanism of Low Salinity Waterflooding in Sandstone Reservoirs. Presented at the SPE Improved Oil Recovery Symposium, Tulsa, Oklahoma, USA, 24-28 April. SPE-129767-MS.

Bennion, D. B., and Bachu, S., 2008. Correlations for the Interfacial Tension between Supercritical Phase CO_2 and Equilibrium Brines at the In Situ Conditions. Presented at the SPE Annual Technical Conference and Exhibition, Denver, Colorado, USA, 21-24 September. SPE-114479-MS.

Callegaro, C., Bartosek, M., Masserano, F. et al. 2013. Opportunity of Enhanced Oil Recovery Low Salinity Water Injection: From Experimental Work to Simulation Study up to Field Proposal. Presented at the EAGE Annual Conference & Exhibition, London, United Kingdom, 10-13 June. SPE-164827-MS.

Calsep. PVTSim Nova 1.1.23 2016 Technical Manual, Calsep, Houston, USA.

Corey, A. T. 1954. The Interrelation Between Gas and Oil Relative Permeability. *Producers Monthly* **19** (1): 38-41.

Fjelde, I., Asen, S. M., and Omekeh, A. 2012. Low Salinity Waterflooding Experiments and Interpretation by Simulations. Presented at the SPE Improved Oil Recovery Symposium, Tulsa, Oklahoma, USA, 14-18 April. SPE-154142-MS.

Ghedan, S. G. 2009. Global Laboratory Experience of CO_2-EOR Flooding. Presented at the SPE/EAGE Reservoir Characterization & Simulation Conference, Abu Dhabi, UAE, 19-21 October. SPE-125581-MS.

Jerauld, G. R., Lin, C. Y., Webb, K. J. et al. 2006. Modeling Low-Salinity Waterflooding. Presented at the SPE Annual Technical Conference and Exhibition, San Antonio, USA, 24-27 September. SPE-102239-MS.

Kevin, L., Yirong, J., Zhijian, D. et al. 1995. The Oil-Water Relative Permeability Behaviour of A Low Permeable Reservoir. Presented at the International Meeting on Petroleum Engineering, Beijing, China, 14-17 November. SPE 30001.

Lager, A., Webb, K., Black,C. et al. 2006. Low Salinity Oil Recovery - An Experimental Investigation. Presented at the International Symposium of the Society of Core Analysis, Trondheim, Norway, 12-16 September. SCA-2006-36.

Lager, A., Webb, K. J., Collins, I. R. et al. 2008. LoSal Enhanced Oil Recovery: Evidence of Enhanced Oil Recovery at the Reservoir Scale. Presented at the SPE/DOE Improved Oil Recovery Symposium, Tulsa, Oklahoma, USA, 19-23 April. SPE-113976-MS.

Lingthelm, D. J., Gronsveld, J., Hofman, J. et al. 2009. Novel Waterflooding Strategy by Manipulation of Injection Brine Composition. Presented at the SPE

EUROPEC/EAGE Conference and Exhibition, Amsterdam, The Netherlands, 8-11 June. SPE-119835-MS.

Mcguire, P. L., Chatham, J. R., Paskvan, F. K. et al. 2005. Low Salinity Oil Recovery: An Exciting Opportunity for Alaska's North Slope. Presented at the SPE Western Regional Meeting, Irvine, California, USA, 20 March - 1 April. SPE-93903-MS.

Mohamad Ibrahim, M. N., and Koederitz, L. F. 2000. Two-Phase Relative Permeability Prediction Using a Linear Regression Model. Presented at the SPE Eastern Regional Meeting, Morgantown, West Virginia, USA, 17-19 October. SPE-65631-MS.

Odeh, A. S. 1959. Effect of Viscosity Ratio on Relative Permeability. *Petroleum Transactions, AIME* **216**: 346-353. SPE-1189-G.

RezaeiDoust, A., Puntervold, T., and Austad, T. 2010. A Discussion of the Low-Salinity EOR Potential for a North Sea Sandstone Field. Presented at the SPE Annual Technical Conference and Exhibition, Florence, Italy, 19-22 September. SPE-134459-MS.

Schlumberger Technology Corporation, Eclipse Reservoir Simulation Suite 2014.1. Technical Description and Reference Manual, Schlumberger Technology Corporation, Houston, USA.

Seccombe, J. C., Lager, A., Webb, K. et al. 2008. Improving Waterflood Recovery: LoSal^{TM} EOR Field Evaluation. Presented at the SPE/DOE Symposium in Improved Oil Recovery, Tulsa, Oklahoma, USA, 20-23 April. SPE-113480-MS.

Skrettingland, K., Holt, T., Tweheyo, M. T. et al. 2010. Snorre Low Salinity Water Injection - Core Flooding Experiments and Single Well Field Pilot. Presented at the SPE Improved Oil Recovery Symposium, Tulsa, Oklahoma, USA, 24-28 April. SPE-129877-MS.

Skrettingland, K., Holt, T., Tweheyo, M. T. et al. 2011. Snorre Low-Salinity-Water Injection-Coreflooding Experiments and Single-Well Field Pilot. *SPE Res Eval & Eng* **14** (2): 182-192. SPE-129877-PA.

Tang, G. Q., and Morrow, N. R., 1999. Influence of Brine Composition and Fines Migration on Crude Oil/Brine/Rock Interactions and Oil Recovery. *Journal of Petroleum Science and Engineering* **24** (2-4): 99-111.

Teklu, T. W., Alameri, W., Graves, R. M. et al. 2014. Low-Salinity Water-Alternating-CO_2 Flooding Enhanced Oil Recovery: Theory and Experiments. Presented at ADIPEC, Abu Dhabi, UAE, 10-13 November. SPE-171767-MS.

Vijapurapu, C. S. and Rao, D. N. 2004. Compositional Effects of Fluids on Spreading, Adhesion and Wettability in Porous Media. *Colloids and Surfaces* **58** (3): 315-326.

Webb, K. J., Black, C. J. J., and Al-Ajee, H. 2004. Low Salinity Oil Recovery - Log Inject Log. presented at the SPE/DOE Symposium in Improved Oil Recovery, Tulsa, Oklahoma, USA, 17-21 April. SPE-89379-MS.